Novel mediators of anti-tumor immunity: dissecting intratumoral immune responses at the single-cell level

Vries, N.L. de

4

γδ T cells are effectors of immune checkpoint blockade in mismatch repair-deficient colon cancers with antigen presentation defects

Natasja L. de Vries[1,2]*, Joris van de Haar[3,4,5]*, Vivien Veninga[3,4]*, Myriam Chalabi[3,6,7]*, Marieke E. Ijsselsteijn[1], Manon van der Ploeg[1], Jitske van den Bulk[1], Dina Ruano[1], Jose G. van den Berg[8], John B. Haanen[3,7], Laurien J. Zeverijn[3,4], Birgit S. Geurts[3,4], Gijs F. de Wit[3,4], Thomas W. Battaglia[3,4], Hans Gelderblom[9], Henk M.W. Verheul[10], Ton N. Schumacher[3,4,11], Lodewyk F.A. Wessels[4,5,12], Frits Koning[2†], Noel F.C.C. de Miranda[1†], Emile E. Voest[3,4†]

[1]Department of Pathology, Leiden University Medical Center, Leiden, the Netherlands. [2]Department of Immunology, Leiden University Medical Center, Leiden, the Netherlands. [3]Department of Molecular Oncology and Immunology, Netherlands Cancer Institute, Amsterdam, The Netherlands. [4]Oncode Institute, Utrecht, the Netherlands. [5]Division of Molecular Carcinogenesis, Netherlands Cancer Institute, Amsterdam, the Netherlands. [6]Gastrointestinal Oncology, Netherlands Cancer Institute, Amsterdam, the Netherlands. [7]Medical Oncology, Netherlands Cancer Institute, Amsterdam, the Netherlands. [8]Department of Pathology, Netherlands Cancer Institute, Amsterdam, the Netherlands. [9]Department of Medical Oncology, Leiden University Medical Center, Leiden, the Netherlands. [10]Department of Medical Oncology, Radboud UMC, Nijmegen, the Netherlands. [11]Department of Hematology, Leiden University Medical Center, Leiden, the Netherlands. [12]Faculty of EEMCS, Delft University of Technology, Delft, the Netherlands. *Co-first authors. †Equal responsible authors.

Manuscript in revision (Nature)

ABSTRACT

DNA mismatch repair deficient (MMR-d) cancers present an abundance of neoantigens that likely underlies their exceptional responsiveness to immune checkpoint blockade (ICB).[1,2] In contrast to other cancer types,[3-5] we observed that 20 out of 21 (95%) MMR-d cancers with genomic inactivation of β2-microglobulin (*B2M*) retained responsiveness to ICB, suggesting the involvement of immune effector cells other than $CD8^+$ T cells in this context. We next identified a strong association between *B2M* inactivation and an increased infiltration by γδ T cells in MMR-d cancers. These γδ T cells were mainly composed of Vδ1 and Vδ3 subsets, and expressed high levels of PD-1, activation markers including cytotoxic molecules, and a broad repertoire of killer-cell immunoglobulin-like receptors (KIRs). *In vitro*, $PD\text{-}1^+$ γδ T cells, isolated from MMR-d colon cancers, exhibited a cytolytic response towards HLA class I-negative MMR-d colon cancer cell lines and *B2M*-knockout patient-derived tumor organoids (PDTOs), which was enhanced as compared to antigen presentation-proficient cells. By comparing paired tumor samples of MMR-d colon cancer patients obtained before and after dual PD-1 and CTLA-4 blockade, we found that ICB profoundly increased the intra-tumoral frequency of γδ T cells in β2m-deficient cancers. Taken together, these data indicate that γδ T cells contribute to the response to ICB in patients with HLA class I-negative, MMR-d colon cancers, and underline the potential of γδ T cells in cancer immunotherapy.

INTRODUCTION

Immune-checkpoint blockade (ICB) targeting the PD-1/PD-L1 and/or CTLA-4 axis provides durable clinical benefit to patients with DNA mismatch repair-deficient (MMR-d)/Microsatellite Instability-High (MSI-H) cancers.[6-9] The exceptional responses of MMR-d/MSI-H cancers to ICB are likely explained by their vast burden of putative neoantigens, which originate from the extensive accumulation of mutations in their genomes.[1,2] This is in line with the current view that PD-1 blockade mainly boosts endogenous antitumor immunity driven by $CD8^+$ T cells, which recognize Human Leukocyte Antigen (HLA) class I-bound neoepitopes on cancer cells.[10-12] However, MMR-d colon cancers frequently lose HLA class I-mediated antigen presentation due to silencing of HLA class I genes, inactivating mutations in β2-microglobulin (*B2M*), or other defects in the antigen processing machinery,[13-16] which may render these tumors resistant to $CD8^+$ T cell-mediated immunity.[3-5,17] Interestingly, early evidence has indicated that β2m-deficient, MMR-d cancers can obtain durable responses to PD-1 blockade,[18] suggesting that immune cell subsets other than $CD8^+$ T cells contribute to these responses.

HLA class I-unrestricted immune cell subsets, capable of tumor killing, include natural killer (NK) cells and γδ T cells. γδ T cells share many characteristics with their αβ T cell counterpart, such as cytotoxic effector functions, but express a distinct TCR composed of a γ and a δ chain. Different subsets of γδ T cells are defined by their TCR δ chain usage, of which those expressing Vδ1 and Vδ3 are primarily "tissue-resident" at mucosal sites, whereas those expressing Vδ2 are mainly found in blood.[19] Both adaptive and innate mechanisms of activation, e.g., through stimulation of their γδ TCR or innate receptors such as NKG2D, DNAM-1, NKp30 or NKp44, have been described for γδ T cells.[20] Killer-cell immunoglobulin-like receptors (KIRs) are expressed by γδ T cells and regulate their activity depending on HLA class I expression in target cells.[21] Furthermore, γδ T cells were found to express high levels of PD-1 in MMR-d colorectal cancers (CRCs), suggesting that these cells may be targeted by PD-1 blockade.[22]

Here, we applied a combination of transcriptomic and imaging approaches for an in-depth analysis of ICB-naïve and ICB-treated MMR-d colon cancers, as well as *in vitro* functional assays, and found evidence indicating that γδ T cells mediate responses to HLA class I-negative, MMR-d tumors during ICB treatment.

RESULTS

B2M-mutant MMR-d cancers retain responsiveness to PD-1 blockade

We evaluated responses to PD-1 blockade therapy in a cohort of 71 patients with MMR-d cancers from various anatomical sites treated in the Drug Rediscovery Protocol (DRUP)[23] in relation to their *B2M* status (**Figure 1A**, **Figure S1A-C**, **Table S1**). Clinical benefit (CB; defined as ≥4 months disease control; the primary outcome of the DRUP) was observed in 20 out of 21 (95%) of patients with $B2M^{MUT}$ tumors *vs* 31 out of 50 (62%) of patients

with *B2M*^{WT} tumors (Fisher's exact test-based two-sided P=0.0038; logistic regression-based P=0.022 and P=0.027, adjusted for tumor mutational burden [TMB], and TMB plus tumor type, respectively; **Figure 1B**). Among patients with *B2M*^{MUT} tumors, 12 out of 21 (57%) experienced a partial response (following RECIST1.1 criteria) and 3 (14%) a complete response. All 44 *B2M* alterations across 21 patients were clonal (**Methods**), consistent with earlier observations in MMR-d cancers[18]. Thirteen out of 21 (62%) patients with *B2M*^{MUT} tumors harbored bi-allelic *B2M* alterations, 4 (19%) potentially bi-allelic alterations, and 4 (19%) non bi-allelic alterations (**Figure 1C**, **Methods**). The latter have also been associated with complete loss of β2m protein expression in MMR-d tumors.[18] Thus, *B2M* alterations are associated with a high clinical benefit rate of PD-1 blockade in patients with MMR-d cancers.

γδ T cells are enriched in *B2M*-mutant MMR-d cancers

To gain insight into immune cell subsets involved in immune responses towards HLA class I-negative MMR-d cancers we used a large cohort of The Cancer Genome Atlas (TCGA) and studied the transcriptomic changes associated with genomic loss of *B2M* in three MMR-d cancer cohorts in colon adenocarcinoma (COAD; n=50 *B2M*^{WT}, n=7 *B2M*^{MUT}), stomach adenocarcinoma (STAD; n=48 *B2M*^{WT}, n=12 *B2M*^{MUT}), and endometrium carcinoma (UCEC; n=118 *B2M*^{WT}, n=4 *B2M*^{MUT}). We found that *B2M* was among the most significantly downregulated genes in *B2M*^{MUT} cancers (two-sided P=3.5 x10^{-4}, Benjamini-Hochberg corrected false discovery rate [FDR]=0.12; **Figure 1D**). Genes encoding components of the HLA class I antigen presentation machinery other than *B2M* were highly upregulated in *B2M*^{MUT} tumors, which may reflect reduced evolutionary pressure on somatic inactivation of these genes in the *B2M*^{MUT} context[18] (**Figure 1D**). Interestingly, we found *TRDV1* and *TRDV3*, which encode the variable regions of the δ1 and δ3 chains of the γδ T cell receptor (TCR), among the most significantly upregulated loci in *B2M*^{MUT} tumors (*TRDV1*: FDR=0.00090; *TRDV3*: FDR=0.0015; **Figure 1D**), regardless of allelic status of the *B2M* alteration (**Figure S1D**). In line with this, the expression level of *TRDV1* and *TRDV3* was higher in *B2M*^{MUT} compared to *B2M*^{WT} MMR-d cancers (Wilcoxon rank sum-based two-sided P=6.5x10^{-8} for all cohorts combined; linear regression-based two-sided P=4.7x10^{-6}, adjusted for tumor type; **Figure 1D-F**). In addition, *B2M*^{MUT} tumors showed overexpression of multiple KIRs (**Figure 1D**), which clustered together with *TRDV1* and *TRDV3* by hierarchical clustering (**Figure S1E**). The expression level of different KIRs (**Table S2**) was higher in *B2M*^{MUT} compared to *B2M*^{WT} MMR-d tumors (Wilcoxon rank sum-based two-sided P=4.4x10^{-6} for all cohorts combined; linear regression-based two-sided P=4.7x10^{-5}, adjusted for tumor type; **Figure 1D-F**). Together, these results suggest that ICB-naïve, *B2M*^{MUT} MMR-d cancers show increased levels of Vδ1 and Vδ3 T cells and (these or other) immune cells expressing KIRs, receptors implied in the recognition and killing of HLA class I-negative cells.

We used marker gene sets (modified from Danaher *et al.*[24]; **Methods**, **Table S2**) to estimate the abundance of a broad set of other immune cell types based on the RNA expression data of the TCGA cohorts. Hierarchical clustering identified a highly and a lowly infiltrated cluster in each of the three tumor types (**Figure 1E**). As compared to the Vδ1/Vδ3 T cell and KIR gene sets, the other marker gene sets showed no or only weak association between

expression level and *B2M* status, indicating that our findings were not solely driven by a generally more inflamed state of *B2M*^{MUT} tumors (**Figure 1E-F**, **Figure S1F**).

We next revisited the DRUP cohort and specifically applied the marker gene sets on RNA expression data. Despite the small patient numbers and high heterogeneity regarding tumor types and biopsy locations of this cohort, we could confirm an increased *TRDV1* and *TRDV3* expression in *B2M*^{MUT} tumors pan-cancer (linear regression-based two-sided P=0.017, adjusted for tumor type and biopsy site; **Figure 1G**, **Figure S1G**, **Methods**). KIR expression was only significantly associated with *B2M* status in CRC (**Figure 1G**). Taken together, *B2M* defects are positively associated with clinical benefit to ICB treatment, as well as infiltration by Vδ1/Vδ3 T cells and expression of KIRs.

Cytotoxic Vδ1 and Vδ3 T cells infiltrate MMR-d colon cancers

To investigate which γδ T cell subsets are present in MMR-d colon cancers and to determine their functional characteristics, we performed single-cell RNA-sequencing (scRNA-seq) on γδ T cells isolated from five MMR-d colon cancers (**Figure S2-3**, **Table S3**). Three distinct Vδ subsets were identified (**Figure 2A**), where Vδ1 T cells were the most prevalent (43% of γδ T cells), followed by Vδ2 (19%) and Vδ3 T cells (11%) (**Figure 2B**). *PDCD1* (encoding PD-1) was predominantly expressed by Vδ1 and Vδ3 T cells, while Vδ1 cells expressed high levels of genes encoding activation markers such as CD39 (*ENTPD1*) and CD38 (**Figure 2C**, **Figure S2B**). Furthermore, proliferating γδ T cells (expressing *MKI67*) were especially observed in the Vδ1 and Vδ3 subsets (**Figure 2C**). Other distinguishing features of Vδ1 and Vδ3 T cell subsets included the expression of genes encoding activating receptors NKp46 (*NCR1*), NKG2C (*KLRC2*), and NKG2D (*KLRK1*) (**Figure 2C**). Interestingly, the expression of several KIRs was also higher in the Vδ1 and Vδ3 subsets as compared to Vδ2 T cells (**Figure 2C**). Almost all γδ T cells displayed expression of genes encoding Granzyme B (*GZMB*), Perforin (*PRF1*), and Granulysin (*GNLY*) (**Figure 2C**). Altogether, these data support a role for γδ T cells in mediating natural cytotoxic antitumor responses in HLA class I-negative MMR-d colon cancers.

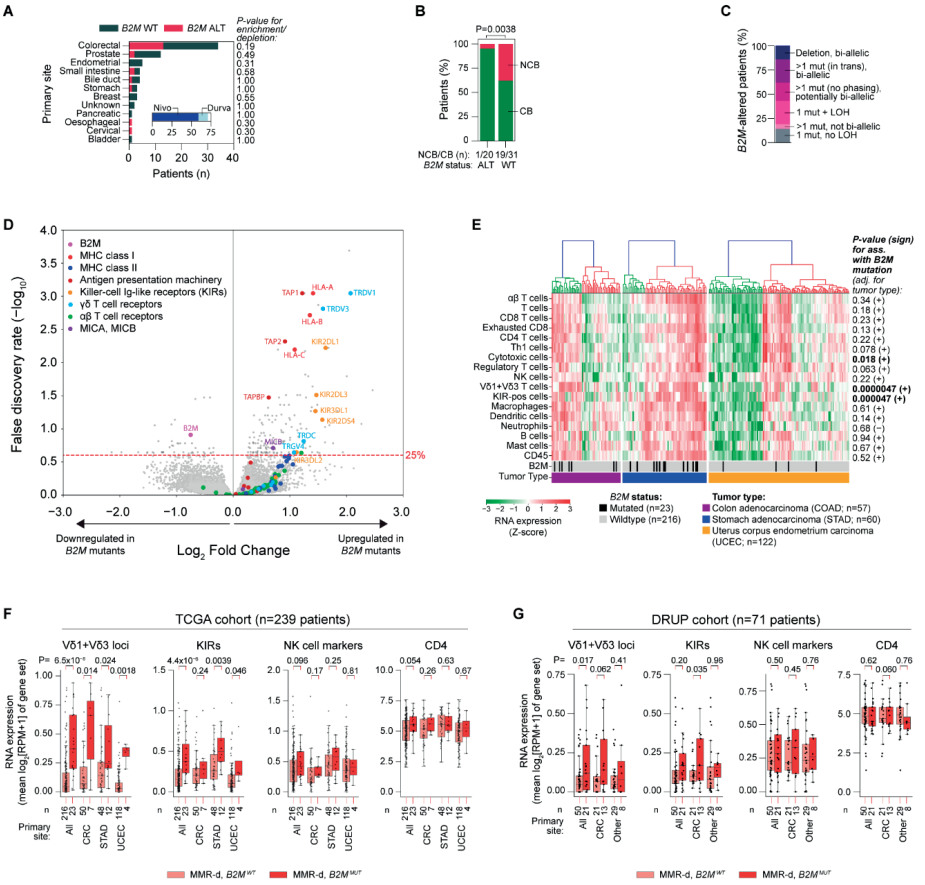

Figure 1. In MMR-d cancers, *B2M* defects are positively associated with clinical benefit to ICB treatment, as well as infiltration by Vδ1/3 T cells and killer-cell immunoglobulin-like receptor (KIR)-expressing cells.
A. The number of patients per primary tumor type for 71 patients in the DRUP with MMR-d cancers and available outcome of ICB therapy. Colors denote patients' *B2M* status (WT: wildtype, gray; ALT: altered, red). Fisher's exact test-based P-values for enrichment/depletion of *B2M* altered cases per primary site are shown. The inset denotes the type of ICB treatment (Nivo: nivolumab, dark blue; Durva: durvalumab, light blue). **B**. The clinical benefit of ICB treatment in the DRUP cohort *vs B2M* status, for the full DRUP cohort. Fisher's exact test-based P-value is shown. **C**. The allelic alteration status of *B2M* in the DRUP cohort. **D**. Volcano plot indicating differential gene expression between *B2M*-mutated *vs* -wildtype MMR-d cancers. The Benjamini Hochberg false discovery rate (FDR) significance threshold of 25% is indicated by the red dashed line. Results were obtained in a combined analysis of all MMR-d cancers of the TCGA COAD (colon adenocarcinoma; n=57 patients), STAD (stomach adenocarcinoma; n=60 patients) and UCEC (uterus corpus endometrial carcinoma; n=122 patients) cohorts, and were adjusted for tumor type. **E**. Heatmap of the expression (Z-score; see color bar) of gene sets whose expression marks infiltration of specific immune cell types in MMR-d cancers of the COAD, STAD and UCEC cohorts of TCGA. Cancers were ranked based on hierarchical clustering, as indicated by the dendrograms (top). The lower two bars indicate the *B2M* mutation status and cancer type. P-values and sign (+ for positive and – for negative) of associations of marker gene expression with *B2M* mutation status are shown on the right. P-values were obtained by ordinary least squares linear regression and adjusted for tumor type. Significant associations (nominal P<0.05) are in bold font. **F**. RNA expression of different immune marker gene sets MMR-d $B2M^{WT}$ (pink), and MMR-d $B2M^{MUT}$ (red) cancers. Results are obtained with the TCGA COAD, STAD and UCEC cohorts, and are shown for all cohorts combined (All), and for each cohort separately. Boxes, whiskers, and dots indicate quartiles, 1.5 interquartile ranges, and individual data points, respectively. Wilcoxon rank sum test-based P-values are shown for MMR-d $B2M^{WT}$ *vs* MMR-d $B2M^{MUT}$ cancers. **G**. As **F**, but for MMR-d cancers in the DRUP cohort. Results are shown for all cancers combined (All), only colorectal cancer (CRC), or all non-CRC cancers (Other).

Next, we applied imaging mass cytometry (IMC) on a cohort of 17 ICB-naïve MMR-d colon cancers (**Table S3**). High levels of γδ T cell infiltration were observed in cancers with β2m defects as compared to β2m-proficient cancers, albeit this difference was not significant (**Figure 2D**). Levels of other immune cells, including NK cells, CD4$^+$ T cells, and CD8$^+$ T cells, were similar between β2m-deficient and -proficient tumors (**Figure 2D**). In β2m-deficient cancers, γδ T cells showed frequent intraepithelial localization and expression of CD103 (tissue-residency), CD39 (activation), granzyme B (cytotoxicity), and Ki-67 (proliferation), as well as PD-1 (**Figure 2D-F**, **Figure S4A**), in line with the scRNA-seq data. Of note, γδ T cells in β2m-deficient cancers showed co-expression of CD103 and CD39 (**Figure S4B**), reported to identify tumor-reactive CD8$^+$ αβ T cells in a variety of cancers[25].

PD-1$^+$ γδ T cells are cytotoxic towards HLA class I-negative colon cancer cells

We next sought to determine whether tumor-infiltrating γδ T cells can recognize and kill CRC cells. We isolated and expanded PD-1$^-$ and PD-1$^+$ γδ T cells from five MMR-d colon cancers (**Figure S5A-C**, **Table S3**). In line with the scRNA-seq data, expanded PD-1$^+$ γδ T cell populations were devoid of Vδ2$^+$ cells and comprised of Vδ1$^+$ or Vδ3$^+$ subsets, whereas PD-1$^-$ fractions contained Vδ2$^+$ or a mixture of Vδ1/Vδ2/Vδ3$^+$ populations (**Figure 3A**, **Figure S5D**). Detailed immunophenotyping of the expanded γδ T cells (**Figure 3A**, **Figure S6A**) showed that all subsets expressed the activating receptor NKG2D, while the surface expression of KIRs was most frequent on PD-1$^+$ γδ T cells (Vδ1 or Vδ3$^+$), in line with the scRNA-seq results of unexpanded populations.

We measured the reactivity of the expanded γδ T cell populations towards HLA class I-negative and HLA class I-positive cancer cell lines (**Figure 3B**, **Figure S6B**). Upon co-culture with the different cancer cell lines, expression of activation markers and secretion of IFNγ was mainly induced in PD-1$^+$ γδ T cells (Vδ1 or Vδ3$^+$) and cell reactivity was most pronounced against HLA class I-negative cell lines (**Figure 3C**, **Figure S6-7**). Reactivity of PD-1$^-$ (enriched in Vδ2$^+$) subsets towards colorectal cancer cell lines was not detected (**Figure 3C**, **Figure S6-7**). To quantify and visualize the differences in killing of CRC cell lines by PD-1$^+$ and PD-1$^-$ γδ T cells, we co-cultured the γδ T cell populations with three CRC cell lines (HCT-15, LoVo, HT-29) in the presence of a fluorescent cleaved-caspase-3/7 reporter to measure cancer cell apoptosis over time (**Figure 3D-E**). This showed pronounced cancer cell apoptosis upon co-culture with PD-1$^+$ γδ T cells (Vδ1 or Vδ3$^+$) as compared to PD-1$^-$ cells, with highest killing of HLA class I-negative HCT-15 cells (**Figure 3E**, **Movie 1-2**). Re-introduction of *B2M* in the *B2M*-deficient HCT-15 and LoVo cells diminished their killing by PD-1$^+$ γδ T cells (Vδ1 or Vδ3$^+$) cells (**Figure S8**).

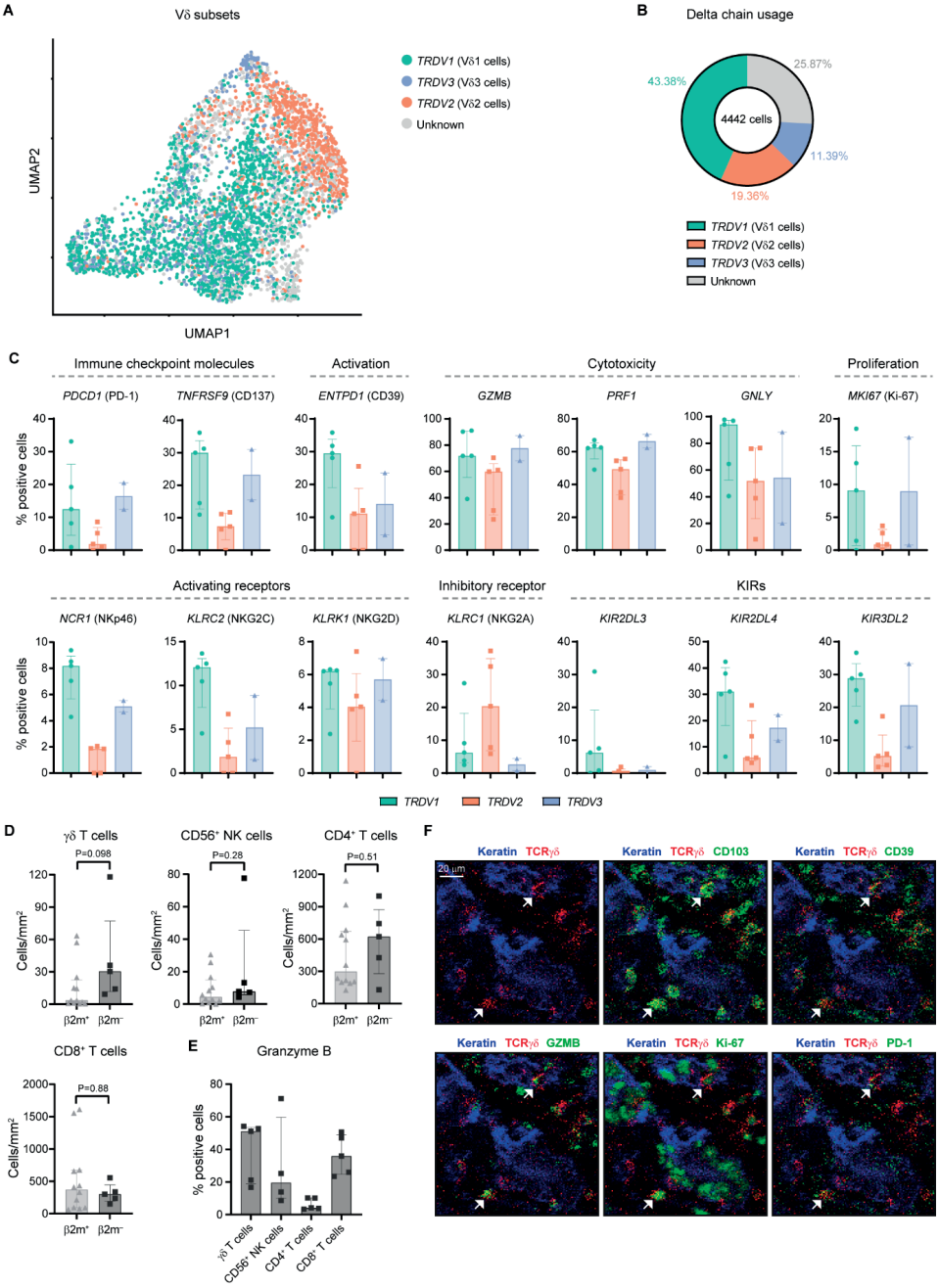

Figure 2. Tumor-infiltrating Vδ1 and Vδ3 T cell subsets display hallmarks of cytotoxic activity in MMR-d colon cancers.

A. UMAP embedding showing the clustering of γδ T cells (n=4442) isolated from MMR-d colon cancers (n=5) analyzed by single-cell RNA-sequencing. Colors represent the TCR Vδ chain usage. The functionally distinct γδ T cell clusters are shown in **Figure S3**. Each dot represents a single cell. **B**. Frequencies of the TCR Vδ chain usage of the γδ T cells (n=4442) analyzed by single-cell RNA-sequencing as a percentage of total γδ T cells. **C**. Frequencies of positive cells for

selected genes across Vδ1 (n=1927), Vδ2 (n=860), and Vδ3 (n=506) cells as percentage of total γδ T cells from each MMR-d colon tumor (n=5) analyzed by single-cell RNA-sequencing. Vδ3 cells were present in two out of five colon cancers. Bars indicate median ± IQR. Each dot represents an individual sample. **D**. Frequencies of γδ T cells, CD56$^+$ NK cells, CD4$^+$ T cells, and CD8$^+$ T cells in treatment-naïve β2m$^+$ (n=12) and β2m$^-$ (n=5) MMR-d colon cancers. Bars indicate median ± IQR. Each dot represents an individual sample. P-values were calculated by Wilcoxon rank sum test. **E**. Frequencies of granzyme B-positive γδ T cells, CD56$^+$ NK cells, CD4$^+$ T cells, and CD8$^+$ T cells in treatment-naïve β2m$^-$ (n=5) MMR-d colon cancers. CD56$^+$ NK cells were present in four out of five β2m$^-$ cancer samples. Bars indicate median ± IQR. Each dot represents an individual sample. **F**. Representative images of the detection of tissue-resident (CD103$^+$), activated (CD39$^+$), cytotoxic (granzyme B$^+$), proliferating (Ki-67$^+$), and PD-1$^+$ γδ T cells by imaging mass cytometry in an treatment-naïve, MMR-d colon cancer with β2m defect.

Next, we established two parental patient-derived tumor organoid lines (PDTOs; **Table S4**) of MMR-d CRC and generated isogenic *B2M^{KO}* lines using CRISPR. Genomic knockout of *B2M* effectively abrogated cell surface expression of HLA class I (**Figure S9**). We exposed two *B2M^{KO}* and their parental *B2M^{WT}* lines to the expanded γδ T cell subsets, and quantified γδ T cell activation by determination of IFNγ expression. Similarly to our cell line data, γδ T cells displayed increased reactivity towards *B2M^{KO}* PDTOs in comparison to the *B2M^{WT}* PDTOs (**Figure 3F-G**). Furthermore, γδ T cell reactivity towards *B2M^{KO}* tumor organoids was preferentially contained within the PD-1$^+$ population of γδ T cells (**Figure 3G**). Thus, lack of HLA class I antigen presentation in MMR-d tumor cells can be effectively sensed by γδ T cells and stimulates their antitumor response.

Expression of NKG2D on γδ T cells decreased during co-culture with target cells (**Figure S10A-B**), suggesting the involvement of the NKG2D receptor in γδ T cell activity. The NKG2D ligands MICA/B and ULBPs were expressed by the cancer cell lines (**Figure 3B**) and the MMR-d CRC PDTOs, irrespective of their *B2M* status (**Figure S9**). To explore which receptor-ligand interactions might regulate the activity of PD-1$^+$ γδ T cells, we performed blocking experiments focused on (i) NKG2D, (ii) DNAM-1, and (iii) γδ TCR signaling. Of these candidates, the only consistent inhibitory effect was observed for NKG2D ligand blocking on cancer cells, which decreased the activation and killing capacity of most PD-1$^+$ γδ T cells (**Figure 3H**, **Figure S10C-D**), confirming the mechanistic involvement of the NKG2D receptor in γδ T cell activation in this context. In addition, blocking NKG2D ligands on MMR-d CRC PDTOs reduced the PDTO-directed tumor reactivity of γδ T cells from CRC94 and CRC134 (**Figure 3I**). Together, these results show that γδ T cell reactivity towards MMR-d tumors is partly dependent on NKG2D/NKG2D-ligand interactions.

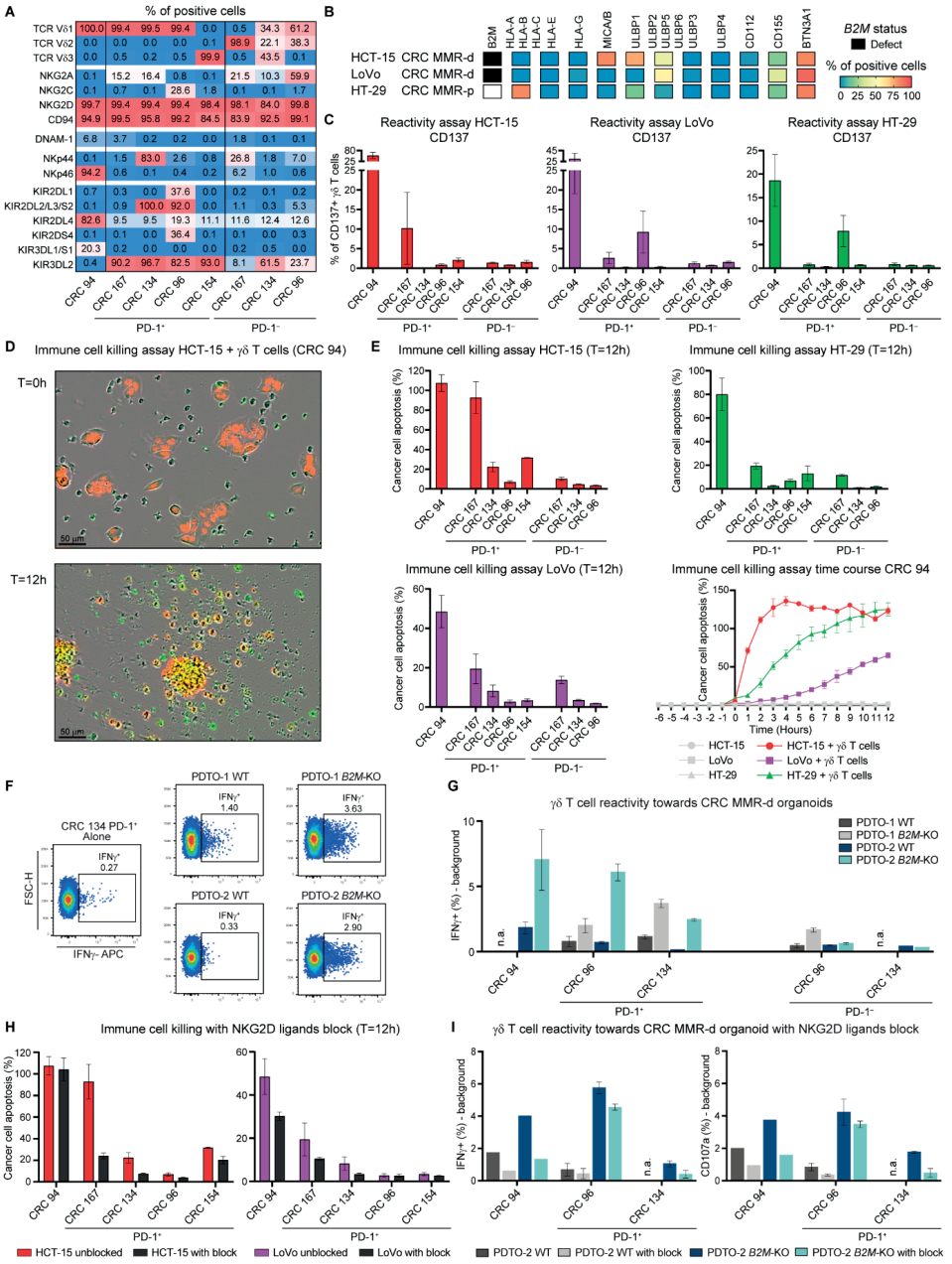

Figure 3. γδ T cells from MMR-d colon cancers show preferential reactivity towards HLA class I-negative cancer cell lines and organoids, which is regulated by NKG2D/NKG2D ligand interactions.

A. Table showing the percentage of positive cells for different TCR Vδ chains, innate immune receptors, and KIRs on expanded PD-1⁺ and PD-1⁻ γδ T cells sorted from MMR-d colon cancers (n=5) as percentage of total γδ T cells. **B**. Diagram showing the *B2M* mutational status and surface expression of HLA class I, NKG2D ligands, DNAM-1 ligands, and butyrophilin on CRC cell lines HCT-15, LoVo, and HT-29. **C**. Bar plots showing the percentage of CD137-positive γδ T cells after 18h co-culture of PD-1⁺ and PD-1⁻ γδ T cells from MMR-d colon cancers (n=5) with HCT-15, LoVo, and HT-29 cells. Medium as negative control and PMA/ionomycin as positive control are shown in **Figure S6**. Bars

indicate mean ± SEM. Data from four (CRC94), three (CRC167, CRC96), or two (CRC134, CRC154) independent experiments, depending on availability of γδ T cells. **D**. Representative images showing the killing of NucLight Red-transduced HCT-15 cells by γδ T cells (unlabeled) from CRC94 in the presence of a green fluorescent caspase-3/7 reagent in the IncuCyte S3. Images are taken immediately after the addition of γδ T cells (T=0) and 12h after. Cancer cell apoptosis is visualized in yellow. **E**. Bar plots showing the quantification of the killing of cancer cell lines by γδ T cells from MMR-d colon cancers (n=5) as in (**D**) after 12h co-culture. Bars indicate mean ± SEM of two wells with two images/well. At lower right, representative time course of cancer cell apoptosis in the presence or absence of γδ T cells derived from CRC94. **F**. Representative flow cytometry plots of PD-1$^+$ γδ T cells from CRC134 indicating IFN-γ expression in unstimulated condition (alone) and upon stimulation with two *B2M^{WT}* and *B2M^{KO}* CRC MMR-d organoids, as specified in the subplot titles. **G**. Histogram showing IFN-γ expression of γδ T cells from MMR-d colon cancers upon stimulation with two *B2M^{WT}* and *B2M^{KO}* CRC MMR-d organoids, as specified in the legend. Background IFN-γ signal of each unstimulated γδ T cell sample was subtracted from tumor organoid-stimulated IFN-γ signal. For all γδ T cell samples, data is shown for two biological replicates except for CRC134 PD-1$^-$ (n=1). Whiskers indicate SEM. **H**. Bar plots showing the quantification of killing of HCT-15 and LoVo cells by γδ T cells from MMR-d colon cancers (n=5) in the presence of blocking antibodies for NKG2D ligands as compared to the unblocked condition after 12h co-culture. Bars indicate mean ± SEM of two wells with two images/well. **I**. Histograms showing IFN-γ (left) and CD107a (right) expression in γδ T cells from MMR-d colon cancers upon stimulation with *B2M^{WT}* PDTO-2 (gray shades) or *B2M^{KO}* PDTO-2 (blue shades), with or without NKG2D ligand blocking (as indicated in the legend). For cultured γδ T cells, data is shown for two biological replicates (n=2) except for CRC94 (n=1). Whiskers indicate SEM.

Activated γδ T cells infiltrate ICB-treated *B2M*-mutant MMR-d colon cancers

We subsequently studied how ICB influences γδ T cell infiltration and activation in MMR-d colon cancers in a therapeutic context. For this purpose, we analysed pre- and post-treatment samples of the NICHE trial[9], in which colon cancer patients were treated with neoadjuvant PD-1 plus CTLA-4 blockade. In line with our observations in the DRUP cohort, 4 out of 5 (80%) *B2M^{MUT}* cancers in the NICHE trial showed a complete pathologic clinical response. IHC analysis confirmed tumor cell-specific loss of β2m protein expression in 4 out of 5 mutated cases. Whereas expression of immune marker gene sets in pre-treatment samples was similar between 5 *B2M^{MUT} vs* 13 *B2M^{WT}* cancers, ICB induced a clear immunological divergence between these two groups (**Figure 4A**). The *B2M^{MUT}* subgroup was most significantly associated with higher post-treatment expression of *TRDV1* and *TRDV3* (Wilcoxon rank sum-based two-sided P=0.0067; **Figure 4A**), followed by higher expression of the general immune cell marker CD45, NK cell-related markers, KIRs, and αβTCRs (Wilcoxon rank sum-based two-sided P=0.016, P=0.016, P=0.027, and P=0.043, respectively; **Figure 4A**, **Figure S11A**). The set of KIRs upregulated upon ICB in *B2M^{MUT}* cancers (**Figure S11B**) was consistent with the sets of KIRs upregulated in *B2M^{MUT}* MMR-d cancers in TCGA (**Figure 1E**), and those expressed by MMR-d tumor-infiltrating γδ T cells (**Figure 2C**). Pre- and post-ICB gene expression levels related to CD4 and CD8 infiltration were not associated with *B2M* status (**Figure 4A**, **Figure 11A**).

To quantify and investigate differences in immune profiles upon ICB treatment, we applied imaging mass cytometry in tissues derived from five *B2M^{MUT}* HLA class I-negative and five *B2M^{WT}* HLA class I-positive cancers pre- and post-ICB treatment. In the ICB-naïve setting, *B2M^{MUT}* MMR-d colon cancers showed higher γδ T cell infiltration as compared to *B2M^{WT}* MMR-d colon cancers (Wilcoxon rank sum-based two-sided P=0.032; **Figure 4B**, **Figure S11C**). No significant differences were observed in the infiltration of other immune cells, such as NK cells, CD4$^+$ T cells, and CD8$^+$ T cells in ICB-naïve *B2M^{MUT} vs B2M^{WT}* MMR-d colon cancers (**Figure 4B**). ICB treatment resulted in major pathologic clinical responses, and residual cancer

cells were absent in most post-ICB samples. All post-ICB tissues showed a profound infiltration of different types of immune cells (**Figure S11D**), of which γδ T cells were the only immune subset significantly higher in ICB-treated *B2M*^{MUT} as compared to *B2M*^{WT} MMR-d colon cancers (Wilcoxon rank sum-based two-sided P=0.016; **Figure 4B**, **Figure S11C**). In the sole *B2M*^{MUT} case that contained cancer cells, the majority of granzyme B^{+} immune cells infiltrating the tumor epithelium were γδ T cells (**Figure 4C**). These γδ T cells displayed co-expression of CD103, CD39, Ki-67, and PD-1 (**Figure S11E-G**). Taken together, these results show that ICB treatment of MMR-d colon cancer profoundly increases the intra-tumoral presence of activated, cytotoxic, and proliferating γδ T cells, especially when these cancers are β2m-deficient, highlighting γδ T cells as effectors of ICB treatment within this context.

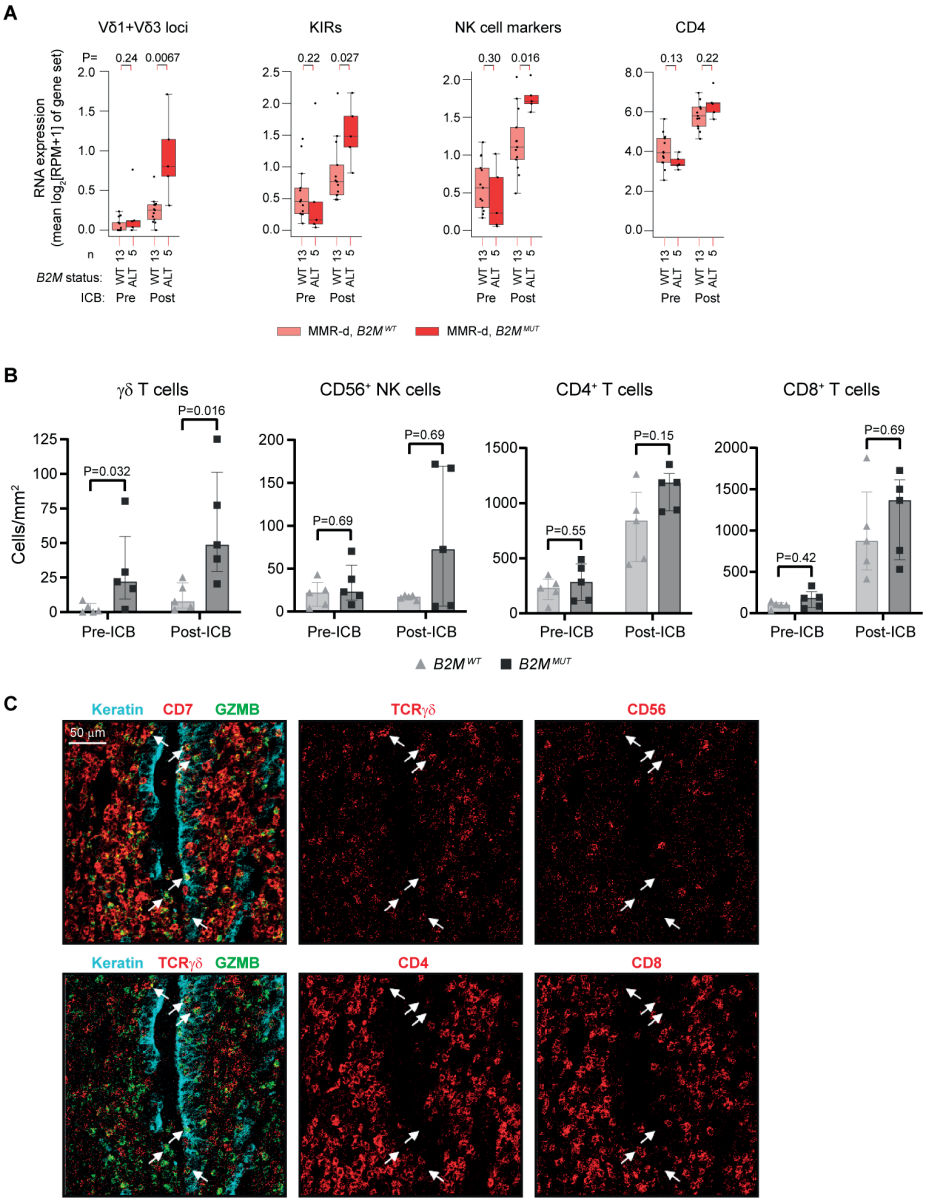

Figure 4. Immune checkpoint blockade (ICB) induces profound infiltration of γδ T cells into MMR-d colon cancers with antigen presentation defects.

A. The RNA expression of different immune marker gene sets in MMR-d *B2M*^{WT} (pink), and MMR-d *B2M*^{MUT} (red) cancers, before (left) and after (right) neoadjuvant ICB in the NICHE study. Boxes, whiskers, and dots indicate quartiles, 1.5 interquartile ranges, and individual data points, respectively. Wilcoxon rank sum test-based P-values are shown for MMR-d *B2M*^{WT} *vs* MMR-d *B2M*^{MUT} cancers. **B**. Frequencies of γδ T cells, CD56^{+} NK cells, CD4^{+} T cells, and CD8^{+} T cells in *B2M*^{WT} (n=5) and *B2M*^{MUT} (n=5) MMR-d colon cancers pre- and post-ICB treatment. Bars indicate median ± IQR. Each dot represents an individual sample. P-values were calculated by Wilcoxon rank sum test. **C**. Representative images of granzyme B-positive γδ T cells infiltrating the tumor epithelium in a *B2M*^{MUT} MMR-d colon cancer upon ICB treatment by imaging mass cytometry.

DISCUSSION

CD8$^+$ αβ T cells are major effectors of ICB[11,12,26] and rely on HLA class I antigen presentation of target cells. Paradoxically, we find that patients with HLA class I defects in MMR-d cancers retain their clinical benefit of ICB, suggesting the involvement of other immune effector cells compensating for the lack of conventional CD8$^+$ T cell immunity in this setting. We show that genomic inactivation of *B2M* in MMR-d colon cancers was associated with: (i) an elevated frequency of activated γδ T cells in ICB-naïve tumors, (ii) an increased presence of tumor-infiltrating γδ T cells upon ICB treatment, (iii) *in vitro* activation of tumor-infiltrating γδ T cells by colorectal cancer cell lines and PDTO, and iv) killing of these tumor cells by γδ T cells, in particular by Vδ1 and Vδ3 subsets expressing PD-1.

Different subsets of γδ T cells exhibit remarkably diverse functions which, in the context of cancer, ranges from tumor-promoting to tumoricidal effects.[27,28] Hence, it is of interest what defines antitumor reactivity of γδ T cells. This study is the first to isolate Vδ1/3-expressing PD-1$^+$ T cells as well as Vδ2-expressing PD-1$^-$ T cells from MMR-d tumor tissues. Our data suggest that especially tumor-infiltrating Vδ1 and Vδ3 T cells can recognize and kill HLA class I-negative MMR-d tumors, whereas Vγ9Vδ2 cells, the most studied and main subset of γδ T cells in the blood, appear to be less relevant within this context. This is in line with other studies showing that the cytotoxic ability of Vδ1 cells generally outperforms their Vδ2 counterparts.[29-33] Of note, cytotoxicity of tumor-infiltrating Vδ3 cells has, to our knowledge, not been reported before. Furthermore, the observation that PD-1$^+$ γδ T cells (Vδ1/Vδ3 phenotype) demonstrated clearly higher levels of antitumor reactivity as compared to their PD-1$^-$ counterparts (Vδ2 phenotype) suggests that, as for CD8$^+$ αβ T cells[34], PD-1 expression may be a marker of antitumor reactivity in γδ T cells.

The mechanisms of activation of γδ T cells are notoriously complex and diverse.[20] Specifically for Vδ1$^+$ cells, NKG2D has been described to be involved in tumor recognition, which is dependent on tumor cell expression of NKG2D ligands MICA/B and ULBPs.[35-37] In our study, MICA/B and ULBPs were highly expressed by the MMR-d CRC cell lines and tumor organoids, and blocking these ligands reduced γδ T cell activation and cytotoxicity. This suggests a role for the activation receptor NKG2D in γδ T cell reactivity towards HLA class I-negative MMR-d tumors. In addition, we detected expression of KIRs primarily on PD-1$^+$ γδ T cells (Vδ1 or Vδ3$^+$ subsets), whose antitumor reactivity and killing was clearly amplified when tumor cells lacked HLA class I.

Our findings have broad implications for cancer immunotherapy. First, our findings provide a basis for novel (combinatorial) immunotherapeutic approaches to further enhance γδ T cell-based antitumor immunity. Second, the presence or absence in tumors of specific γδ T cell subsets (e.g. Vδ1 or Vδ3) may help to define patients (un)responsive to ICB, especially in the case of MMR-d cancers and other malignancies with frequent HLA class I defects, like stomach adenocarcinoma[38] and Hodgkin lymphoma[39]. Third, our results suggest that MMR-d cancers and other tumors with HLA class I defects may be particularly attractive

targets for Vδ1 or Vδ3 T cell-based cellular therapies.

Although we have provided detailed and multidimensional analyses, it is likely that γδ T cells are not the only factor driving ICB responses in HLA class I-negative MMR-d CRC tumors. In this context, other HLA class I-independent immune subsets, like NK cells and (neoantigen-specific) $CD4^+$ T cells may also contribute. The latter were shown to play an important role in response to ICB (as reported in murine *B2M*-deficient MMR-d cancer models[40]), and may also support γδ T cell-driven responses. Of note, no equivalent subset to Vδ1 or Vδ3 T cells has been identified in mice which complicates their investigation in *in vivo* models. In conclusion, our results provide strong evidence that γδ T cells are cytotoxic effector cells of ICB treatment in HLA class I-negative MMR-d colon cancers, with implications for further exploitation of γδ T cells in cancer immunotherapy.

METHODS

TCGA data

RNA expression data (raw counts and Fragments Per Kilobase of transcript per Million mapped reads upper quartile FPKM-UQ) of the colon adenocarcinoma (COAD), stomach adenocarcinoma (STAD) and Uterus Corpus Endometrium Carcinoma (UCEC) cohorts of The Cancer Genome Atlas (TCGA) Research Network were downloaded via the GDC data portal (https://portal.gdc.cancer.gov) on April10th, 2019. Of these cohorts, mutation, copy number, purity and ploidy data were downloaded from GDC on November 11th, 2021, as the controlled access ABSOLUTE[41]-annotated MAF file (mutations), SNP6 whitelisted copy number segments file (copy numbers), and ABSOLUTE purity/ploidy file of the TCGA PanCanAtlas project[42]. Mismatch repair-deficiency status was obtained from Thorsson *et al.*[43] (TCGA Subtype = GI.HM-indel or UCEC.MSI).

DRUP data

A detailed description of the DRUP, including details on patient accrual, study design, oversight and endpoints has been published earlier in this journal[23]. Briefly, the DRUP is a national, non-randomized multi-drug and multi-tumor study in the Netherlands, in which patients receive off-label drugs registered for other treatment indications. We analyzed 71 patients with MMR-d cancers treated with PD-1 blockade in the DRUP[23] who had (i) clinical follow-up ≥16 weeks after start of PD-1 blockade treatment (i) WGS data passing standard quality controls (as defined before, including a sequencing-based tumor purity ≥20%[44]), (ii) available RNA-seq data (**Table S1**). MMR-d status was determined using routine diagnostics at the hospital of patient accrual and confirmed by WGS, based on an MSIseq[45] score >4, which represents a predefined threshold[44]. Clinical benefit was defined as disease control ≥16 weeks, consistent with the primary endpoint of the DRUP[23]. For genomics and transcriptomics analyses, fresh frozen tumor biopsies were obtained at baseline (i.e. prior to PD-1 blockade). WGS analysis (median depths ~100X and ~40X for tumor and normal, respectively) and bioinformatics were performed as previously described[23,44], with an optimized pipeline based on open source tools, which is freely available on GitHub (https://github.com/hartwigmedical/pipeline5). The tumor mutational burden per Mb (TMB) was determined by counting the genome-wide number of mutations (SNVs, MNVs, and indels) and dividing this number by the number of mega bases sequenced. For RNA-seq analysis, we extracted total RNA using the QIAGEN QIAsymphony RNA kit (cat nr 931636). Samples with approximately 100ng total RNA were prepared with KAPA RNA Hyper + RiboErase HMR (cat nr 8098131702) and RNA libraries were paired end sequenced on the Illumina NextSeq550 platform (2x75bp) or Illumina NovaSeq6000 platform (2x150bp). Raw RNA reads (FASTA files) were aligned to the human reference genome (GRCh38) with STAR software[46], version 2.7.7a, using default settings in two-pass mode.

NICHE study sequencing data

Raw RNA reads (FASTA files) of our recently published NICHE study[9] (ClinicalTrials.gov: NCT03026140) were generated as described in the original publication and aligned to the human reference genome (GRCh38) with STAR software[46], version 2.7.7a, using default settings in two-pass mode. For gene expression quantification, we used the gencode.v35.annotation.gtf annotation file. Somatic mutation data were obtained from DNA sequencing of pre-treatment tumor biopsies and matched germline DNA, as described in the original publication[9].

***B2M* status**

Consistent with the notion that both bi-allelic and mono-allelic non-synonymous *B2M* mutations are strongly associated with tumor-specific loss of β2m protein expression,[18] we considered all tumors with at least one somatic, non-synonymous *B2M* mutation to be "*B2M* mutant". As none of the *B2M* mutant tumors in TCGA harbored *B2M* copy number gains or losses, loss of heterozygosity (LOH) of *B2M* could be easily assessed by a simple calculation estimating the mutation's copy number:

$$Mut_{CN} = round(2 * \frac{VAF}{purity})$$

Here, Mut_{CN} represents the estimated mutation's copy number (rounded to an integer value), VAF represents the variant allele frequency of the mutation and purity equals the (ABSOLUTE[41]-based) tumor cell fraction of the sample.
A Mut_{CN} equal to 2 was considered consistent with LOH, as the most parsimonious explanation of such a result is the scenario in which all tumor-derived reads spanning the region of the *B2M* mutation harbor the mutation and none of the tumor-derived reads are wildtype.

In analyses of patients in the DRUP, LOH of *B2M* mutations was determined as an integrated functionality of PURPLE v2.34[47]. When multiple *B2M* mutations were present within a sample, we manually phased the mutations through inspection of the *B2M*-aligned reads using the Integrative Genomics Viewer (IGV)[48]. Here, mutations were only phased in case single reads were observed spanning the genomic locations of both mutations. We divided patients with multiple *B2M* mutations into three subgroups:

1. Bi-allelic, if:
    a. The multiple mutations were in trans AND the (integer) sum of the mutation copy numbers equaled (or exceeded) the integer copy number of the *B2M* gene (for mutations in cis, only one of these mutations was considered in the calculation); OR
    b. At least one of the mutations showed LOH.
2. Potentially bi-allelic, if:
    a. The multiple mutations affected too distant genomic locations and could therefore not be phased AND the (integer) sum of the mutation copy numbers equaled (or exceeded) the integer copy number of the *B2M* gene (for mutations in cis, only one of these mutations was considered in the calculation) AND none of the mutations showed LOH.
3. Not bi-allelic, if:
    a. The (integer) sum of the mutation copy numbers was smaller than the integer copy number of the *B2M* gene (for mutations in cis, only one of these mutations was considered in the calculation) AND none of the mutations showed LOH.

In these analyses, mutations were considered to be subclonal in case the probability of subclonality was >0.5 (the situation in which a mutation is more likely subclonal than clonal), as determined by PURPLE v2.34[47].

Association of *B2M* status with outcome and tumor characteristics
To test if somatic *B2M* alterations were associated with the clinical benefit rate of patients with MMR-d tumors treated with ICB in the DRUP, we used a Fisher's exact test (using the Python package Scipy[49]) for unadjusted analyses and logistic regression (as implemented by the Python package "Statsmodels" (https://pypi.org/project/statsmodels/), version 0.10.1) for analyses adjusted for the (continuous) tumor mutational burden per Mb (TMB) and/or the primary site of the tumor. The association of *B2M* status with TMB was tested using Scipy's Wilcoxon rank sum test. Associations of *B2M* status with the primary site of the tumor or the biopsy location was tested by Scipy's Fisher's exact test.

Association of TMB with ICB treatment outcome
For the DRUP cohort, the association of clinical benefit with TMB was tested using Statsmodels' Wilcoxon rank sum test.

Differential expression analysis

Differential RNA expression of genes was tested in R using EdgeR[50], Limma[51] and Voom[52]. Raw read counts were filtered by removing lowly expressed genes. Normalization factors were calculated using EdgeR, in order to transform the raw counts to $\log_2$ counts per million reads (CPM) and calculate residuals using Voom. Voom was then used to fit a smoothened curve to the √(residual standard deviation) by average gene expression, which was then plotted for visual inspection to confirm that the appropriate threshold was used for filtering of lowly expressed genes (defined as the minimal amount of filtering necessary to overcome a dipping mean-variance trend at low counts). Next, Limma was used to calculate differential expression of genes based on a linear model fit, considering the smoothened curve for sample weights, and empirical Bayes smoothing of standard errors. False discovery rates (FDRs) were calculated by Benjamini-Hochberg correction of the obtained p-values.

TCGA data

Using TCGA data, we calculated differential expression between tumors with and without high impact mutations in *B2M*, adjusting for tumor type and tumor mutational burden (TMB), using the following design formula: expression ~ Primary_Site + TMB + B2M_status (+ intercept by default), for which Primary_Site was a three-leveled factor (COAD, STAD, or UCEC), TMB was a continuous variable ($\log_{10}$[exome-wide number of mutations]) and B2M_status was a two-leveled factor (mutated, or wildtype).

NICHE study data

Using NICHE study data, we calculated differential expression between pre- and post-ICB treatment. In order to respect the paired nature of these data, we used the following design formula: expression ~ Patient + ICB (+ intercept by default), for which Patient was a factor for each individual patient and ICB was a two-leveled factor (ICB-treated yes/no).

Immune marker gene set expression analysis

To utilize RNA-seq data in order to obtain a relative estimate of the infiltration of specific immune cell types within tumors of TCGA, we summed the $\log_2$(FPKM-UQ+1) expression of genes that are specifically expressed in the immune cell types of interest. To this end, we used the marker gene sets published by Danaher *et al.*[24], and extended this by (i) *CD4* as $CD4^+$ T cell marker gene, (ii) *TRDV1* and *TRDV3* as γδ1/3T cell marker genes, and (iii) a killer-cell Ig-like receptor (KIR) gene set (comprised of all genes whose name starts with "KIR" and whose name contains "DL" or "DS". We excluded the gene set "NK CD56dim cells" of Danaher *et al*. (comprising IL21R, KIR2DL3, KIR3DL1, and KIR3DL2) from our analyses, as three out of four genes within this set were KIRs and hence this set showed high collinearity/redundancy to our full KIR gene set. As *XLC1* and *XLC2* are highly expressed by tumor-infiltrating γδ T cells, these genes were removed from the NK cell marker gene set and replaced by *KLRF1*, which encodes the well-established NK cell marker NKp80. The resulting gene set consisted of *NCR1* and *KLRF1*, encoding the well-established NK cell markers NKp46 and NKp80, respectively. Finally, we reduced the "cytotoxic cells" marker gene set of Danaher et al. to those genes in the set encoding cytotoxic molecules (GZMA, GZMB, GZMH, PRF1, GNLY, CTSW). The final collection of our marker gene sets can be found in **Table S2**.

Association of immune cell marker gene set expression with *B2M* alteration status (alteration yes/no) was calculated as follows:

1. For TCGA study-based analyses, we used (i) the Wilcoxon rank sum test (for unadjusted analyses) and (ii) ordinary least squares linear regression (for analyses adjusted for tumor type), using a similar design formula as for the differential gene expression analysis.
2. For DRUP cohort-based analyses, we used a linear mixed effects model (as implemented by the "lmer" function of the R package "lme4"), adjusting for tumor type and biopsy site as

random effects, using the following design formula: expression ~ B2M_status + (1|tumor_type) + (1|biopsy_site) (+ intercept by default).

3. For NICHE study-based analyses, we used the Wilcoxon rank sum test (for unadjusted analyses).

Hierarchical clustering

Hierarchical clustering of expression profiles of individual genes or immune marker gene sets of TCGA cohorts was performed on Z-score-transformed $\log_2$(RPM+1) expression values, using the Python package Scipy[49], with Euclidean distance as distance metric and using the Ward variance minimization algorithm. Here, we used default settings with one exception: for visualization purposes, the color threshold was halved in the TCGA-based clustering of individual genes.

Patient samples

The DRUP was designed and conducted on behalf of the Center for Personalized Cancer Treatment (CPCT; clinicaltrials.gov: NCT02925234). This study was approved by the Medical Ethical Committee of the Netherlands Cancer Institute in Amsterdam, and was conducted in accordance with good clinical practice guidelines and the Declaration of Helsinki's ethical principles for medical research. Written informed consent was obtained from all study subjects. In addition, primary colon cancer tissues from a total of 17 patients with colon cancer who underwent surgical resection of their tumor at the Leiden University Medical Center (LUMC, the Netherlands; **Table S3**) were used for scRNA-seq, imaging mass cytometry, and functional assays. No patient with a previous history of inflammatory bowel disease was included. This study was approved by the Medical Ethical Committee of the Leiden University Medical Center (protocol P15.282), and patients provided written informed consent. In addition, primary colon cancer tissues from 10 patients with colon cancer included in the NICHE study (NCT03026140)[9] carried out at the Netherlands Cancer Institute (NKI, the Netherlands) were used for this study. All specimens were anonymized and handled according to the ethical guidelines described in the Code for Proper Secondary Use of Human Tissue in the Netherlands of the Dutch Federation of Medical Scientific Societies.

Processing of colorectal cancer tissues

Details on the processing of colorectal tumor tissues have been described previously[22]. In short, macroscopic sectioning from the lumen to the most invasive area of the tumor was performed. Tissues were collected in IMDM+Glutamax medium (Gibco) complemented with 20% fetal calf serum (FCS) (Sigma-Aldrich), 1% pen/strep (Gibco) and fungizone (Gibco), and 0.1% ciprofloxacin (provided by apothecary LUMC) and gentamicin (Invitrogen), and immediately cut into small fragments in a petri dish. Enzymatical digestion was performed with 1 mg/mL collagenase D (Roche Diagnostics) and 50 µg/mL DNase I (Roche Diagnostics) in 5 mL of IMDM+Glutamax medium for 30 min at 37°C in gentleMACS C tubes (Miltenyi Biotec). During and after incubation, cell suspensions were dissociated mechanically on the gentleMACS Dissociator (Miltenyi Biotec). Cell suspensions were filtered through a 70-µm cell strainer (Corning), washed in IMDM+Glutamax medium with 20% FCS, 1% pen/strep, and 0.1% fungizone, and cell count and viability were determined with the Muse Count & Viability Kit (Merck) on the Muse Cell Analyzer (Merck). Based on the number of viable cells, cells in IMDM+Glutamax medium were cryopreserved in liquid nitrogen until time of analysis complemented 1:1 with 80% FCS and 20% dimethyl sulfoxide (DMSO) (Merck).

Immunohistochemical detection of MMR, β2m, and HLA class I proteins

Tumor MMR status was determined by immunohistochemical detection of PMS2 (anti-PMS2 antibodies; clone EP51, DAKO) and MSH6 (anti-MSH6 antibodies; clone EPR3945, Abcam) proteins[53]. MMR-deficiency was defined as the lack of expression of at least one of the MMR-proteins in the presence of an internal positive control. Tumor β2m status was determined by immunohistochemical detection of β2m (anti-β2m antibodies; clone EP2978Y, Abcam). Immunohistochemical detection of HLA class I

expression on tumors was performed with HCA2 and HC10 monoclonal antibodies (Nordic-MUbio), and classified as HLA class I positive, weak, or loss as described previously[16]. For the tumor samples from the NICHE study, immunohistochemistry of the FFPE tissue was performed on a BenchMark Ultra autostainer (Ventana Medical Systems). Briefly, paraffin sections were cut at 3 µm, heated at 75°C for 28 min, and deparaffinized in the instrument with EZ prep solution (Ventana Medical Systems). Heat-induced antigen retrieval was carried out using Cell Conditioning 1 (CC1, Ventana Medical Systems) for 32 min at 95°C (HC10) or 64 min at 95°C (β2m and HCA2). HLA Class I Heavy Chain expression was detected using clone HCA2 (1/5000 dilution, 60 min at RT; Nordic-Mubio) and clone HC10 (dilution 1/20000, 32 min at 37°C; Nordic-Mubio). β2m was detected using clone D8P1H (dilution 1/1500, 60 min at RT; Cell Signaling). Bound antibody was detected using the OptiView DAB Detection Kit (Ventana Medical Systems). Slides were counterstained with Hematoxylin and Bluing Reagent (Ventana Medical Systems). A PANNORAMIC® 1000 scanner from 3DHISTECH was used to scan the slides at a 40x magnification.

Sorting of γδ T cells from colon cancer and single-cell RNA-sequencing

scRNA-seq was performed on sorted γδ T cells from colon cancers (MMR-d) of five patients from the LUMC in the presence of hashtag oligo (HTOs) for sample ID and antibody-derived tags (ADTs) for CD45RA and CD45RO protein expression by CITE-seq[54]. Cells were thawed, rest at 37°C in IMDM (Lonza)/20% FCS for 1h, followed by incubation with human Fc receptor block (BioLegend) for 10 min at 4°C. Thereafter, cells were stained with cell surface antibodies (1:50 anti-CD3-PE [clone SK7, BD Biosciences], 1:160 anti-CD45-PerCP-Cy5.5 [clone 2D1, eBioscience], 1:200 anti-CD7-APC [clone 124-1D1, eBioscience], 1:60 anti-EPCAM-FITC [clone HEA-125, Miltenyi], 1:80 anti-TCRγδ-BV421 [clone 11F2, BD Biosciences], and a 1:1000 near-infrared viability dye [Life Technologies]), 1 µg of TotalSeq-C anti-CD45RA (clone HI100, BioLegend) and 1 µg of anti-CD45RO (clone UCHL1, BioLegend) antibodies, and 0.5 µg of a unique TotalSeq-C CD298/β2M hashtag antibody (clone LNH-94/2M2, BioLegend) for each sample (n=5) for 30 min at 4°C. Cells were washed three times in FACS buffer (PBS (Fresenius Kabi)/1% FCS) and kept cold and dark until cell sorting. Compensation was carried out with CompBeads (BD Biosciences) and ArC reactive beads (Life Technologies). Single, live $CD45^+$ $EPCAM^-$ $CD3^+$ $TCR\gamma\delta^+$ cells from five colorectal tumors (MMR-d) were sorted on a FACS Aria III 4L (BD Biosciences). After sorting, the samples were pooled.

scRNA-seq libraries were prepared using the Chromium Single Cell 5' Reagent Kit v1 chemistry (10X Genomics) following the manufacturer's instructions. The construction of 5' Gene Expression libraries allowed the identification of γδ T cell subsets according to Vδ and Vγ usage. Libraries were sequenced on a HiSeq X Ten using paired-end 2x150 bp sequencing (Illumina). Reads were aligned to the human reference genome (GRCh38) and quantified using Cell Ranger (version 3.1.0). Downstream analysis was performed using Seurat (version 3.1.5) according to the author's instructions[55]. Briefly, cells that had less than 200 detected genes and genes that were expressed in less than six cells were excluded. The resulting 5669 cells were demultiplexed based on HTO enrichment using the MULTIseqDemux algorithm[56]. Next, cells with a mitochondrial gene content greater than 10% and cells with outlying numbers of expressed genes (>3000) were filtered out from the analysis, resulting in a final dataset of 4442 cells. Data were normalized using the 'LogNormalize' function from Seurat with scale factor 10,000. Variable features were identified using the 'FindVariableFeatures' function from Seurat returning 2,000 features. We then applied the 'RunFastMNN' function from SeuratWrappers split by sample ID to adjust for potential batch-derived effects across samples[57]. Uniform manifold approximation (UMAP)[58] was used to visualize the cells in a two-dimensional space, followed by the 'FindNeighbors' and 'FindClusters' functions from Seurat. Data were scaled and heterogeneity associated with mitochondrial contamination was regressed out. Cell clusters were identified by performing differentially expressed gene analysis with the 'FindAllMarkers' function with min.pct and logfc.threshold at 0.25. Percentage of *TRDV1* (Vδ1), *TRDV2* (Vδ2), or *TRDV3* (Vδ3) positive cells was determined as the percentage of all cells with an expression level of >1, while <1 for the other TCR Vδ chains. CRC96, 134 and 167 had less than ten $TRDV3^+$ cells,

and were not included in the Vδ3 analysis. Transcripts of Vδ4 *(TRDV4),* Vδ5 *(TRDV5),* and Vδ8 *(TRDV8)* cells were not detected. Percentage of *TRGV1* (Vγ1) – *TRGV11* (Vγ11) positive cells was determined as the percentage of all cells with an expression level of >1, while <1 for the other TCR Vγ chains. Percentage of cells positive for a certain gene was determined as all cells with an expression level of >1.

Imaging mass cytometry staining and analysis

Imaging mass cytometry (IMC) was performed on ICB-naïve colon cancer tissues (MMR-d) of 17 patients from the LUMC, of which four HLA class I-positive, eight HLA class I-defect, and five β2m-defect (**Table S1**). In addition, IMC was performed on ICB-treated colon cancer tissues (MMR-d) of ten patients from the NKI, of which five $B2M^{WT}$ and five $B2M^{MUT}$. Antibody conjugation and immunodetection were performed following the methodology published previously by Ijsselsteijn *et al.*[59]. Four-µm FFPE tissue were incubated with 41 antibodies in four steps. First, sections were incubated with anti-CD4 and anti-TCRδ overnight at RT, which were subsequently detected using metal-conjugated secondary antibodies (goat anti-rabbit IgG and goat anti-mouse IgG, respectively; Abcam). Second, sections were incubated with 20 antibodies (**Table S3**) for five hours at RT. Third, sections were incubated overnight at 4°C with the remaining 19 antibodies (**Table S3**). Fourth, sections were incubated with 0.125 µM Cell-ID intercalator-Ir (Fluidigm) to detect the DNA, and stored dry until measurement. For each sample, six 1000x1000µm regions were selected based on consecutive Haematoxylin and Eosin (H&E) stains and ablated using the Hyperion Imaging system (Fluidigm). Data was acquired with the CyTOF Software (version 7.0) and exported with MCD Viewer (version 1.0.5). Data was normalized using semi-automated background removal in ilastik[60], version 1.3.3, to control for variations in signal-to-noise between FFPE sections as described previously[61]. Thereafter, the phenotype data was normalized at pixel level. Cell segmentation masks were created for all cells in ilastik and CellProfiler[62], version 2.2.0. In ImaCytE[63], version 1.1.4, cell segmentation masks and normalized images were combined to generate single-cell FCS files containing the relative frequency of positive pixels for each marker per cell. Cells forming visual neighborhoods in a t-distributed Stochastic Neighbor Embedding (t-SNE)[64] embedding in Cytosplore[65], version 2.3.0, were grouped and exported as separate FCS files. The resulting subsets were imported back into ImaCyte and visualized on the segmentation masks. Expression of immunomodulatory markers was determined as all cells with a relative frequency of at least 0.2 positive pixels per cell. Differences in cells/mm^2 were calculated by Mann-Whitney tests in Graphpad Prism (version 9.0.1).

Sorting of γδ T cells from colon cancer and cell culturing

γδ T cells from colon cancers (MMR-d) of five patients from the LUMC were sorted for cell culture. Cells were thawed and rest at 37°C in IMDM (Lonza)/10% nHS for 1h. Thereafter, cells were incubated with human Fc receptor block (BioLegend) and stained with cell surface antibodies (1:20 anti-CD3-Am Cyan [clone SK7, BD Biosciences], 1:80 anti-TCRγδ-BV421 [clone 11F2, BD Biosciences], and 1:30 anti-PD-1-PE [clone MIH4, eBioscience] for 45 min at 4°C together with different additional antibodies for immunophenotyping (including 1:10 anti-CD103-FITC [clone Ber-ACT8, BD Biosciences], 1:200 anti-CD38-PE-Cy7 [clone HIT2, eBioscience], 1:60 anti-CD39-APC [clone A1, BioLegend], 1:20 anti-CD45RA-PE-Dazzle594 [clone HI100, Sony], 1:20 anti-CD45RO-PerCP-Cy5.5 [clone UCHL1, Sony], 1:40 anti-TCRαβ-PE-Cy7 [clone IP26, BioLegend], 1:50 anti-TCRVδ1-FITC [clone TS8.2, Invitrogen], or 1:200 anti-TCRVδ2-PerCP-Cy5.5 [clone B6, BioLegend]. A 1:1000 live/dead fixable near-infrared viability dye (Life Technologies) was included in each staining. Cell were washed three times in FACS buffer (PBS/1% FCS) and kept cold and dark until cell sorting. Compensation was carried out with CompBeads (BD Biosciences) and ArC reactive beads (Life Technologies). Single, live CD3$^+$ TCRγδ$^+$ PD-1$^+$ and PD-1$^-$ cells from five colorectal tumors (MMR-d) were sorted on a FACS Aria III 4L (BD Biosciences). For CRC94 all γδ T cells were sorted due to the low number of PD-1$^+$ cells. γδ T cells were sorted in medium containing feeder cells (1x10^6/mL), PHA (1 µg/mL; Thermo Fisher Scientific), IL-2 (1000 IU/mL; Novartis), IL-15 (10 ng/mL; R&D Systems), gentamicin (50 µg/mL), and fungizone (0.5 µg/mL). Sorted γδ T cells were expanded in the presence of 1000 IU/mL IL-2 and 10 ng/mL IL-15 for three-four weeks. Purity and phenotype of γδ T cells were assessed by flow cytometry. We obtained a >170,000-fold increase in 3-4

weeks of expansion of γδ T cells (**Figure S5C**).

Immunophenotyping of expanded γδ T cells by flow cytometry

Expanded γδ T cells from colon tumors were analyzed by flow cytometry for the expression of TCR Vδ chains, NKG2 receptors, NCRs, KIRs, tissue-residency/activation markers, cytotoxic molecules, immune checkpoint molecules, cytokine receptors, and Fc receptors. Briefly, cells were incubated with human Fc receptor block (BioLegend) and stained with cell surface antibodies (**Table S4**) for 45 min at 4°C, followed by three washing steps in FACS buffer (PBS/1% FCS). Granzyme B and perforin were detected intracellularly using Fixation Buffer and Intracellular Staining Permeabilization Wash Buffer (BioLegend). Compensation was carried out with CompBeads (BD Biosciences) and ArC reactive beads (Life Technologies). Cells were acquired on a FACS LSR Fortessa 4L (BD Biosciences) running FACSDiva software version 9.0 (BD Biosciences). Data were analyzed with FlowJo software version 10.6.1 (Tree Star Inc).

Cancer cell line models and culture

Human colorectal adenocarcinoma cell lines HCT-15 (MMR-d), LoVo (MMR-d), HT-29 (MMR-p), SW403 (MMR-p), and SK-CO-1 (MMR-p) as well as HLA class I deficient human leukemia cell line K-562 and Burkitt lymphoma cell line Daudi were used as targets for reactivity and immune cell killing assays. The cell lines were authenticated by STR profiling and tested for mycoplasma. HCT-15, LoVo, HT-29, K-562, and Daudi cells were maintained in RPMI (Gibco)/10% FCS. SW403 and SK-CO-1 were maintained in DMEM/F12 (Gibco)/10% FCS. All adherent cell lines were trypsinized before passaging. The *B2M*-knockin HCT-15 and LoVo cell lines were generated by using the *B2M* plasmid (pLV[Exp]-EF1A>hB2M[NM_004048.4](ns):T2A:Puro), produced in lentivirus according to standard methodology. Cells were selected using puromycin and afterwards FACS-sorted based on HLA-A/B/C expression using 1:100 anti-HLA-A/B/C-FITC [clone W6/32, eBioscience].

Organoid models and culture

Tumor organoids were derived from MMR-d CRC tumor of two patients via resection from the colon, tumor organoid 1, or peritoneal biopsy, tumor organoid 2 (**Table S2**). Establishment of the respective organoid lines from tumor material was performed as previously reported[66,67]. Briefly, tumor tissue was mechanically dissociated and digested with 1.5 mg/mL of collagenase II (Sigma-Aldrich), 10 µg/mL of hyaluronidase type IV (Sigma-Aldrich), and 10 µM Y-27632 (Sigma-Aldrich). Cells were embedded in Cultrex® RGF BME Type 2 (cat no. 3533-005-02, R&D systems) and placed in a 37°C incubator for 20 min. Human CRC organoids medium is composed of Ad-DF+++ (Advanced DMEM/F12 (GIBCO) supplemented with 2 mM Ultraglutamine I (Lonza), 10 mM HEPES (GIBCO), and 100/100 U/mL Penicillin/Streptomycin (GIBCO), 10% Noggin-conditioned medium, 20% R-spondin1- conditioned medium, 1x B27 supplement without vitamin A (GIBCO), 1.25 mM N- acetylcysteine (Sigma-Aldrich), 10 mM nicotinamide (Sigma-Aldrich), 50 ng/mL human recombinant EGF (Peprotech), 500 nM A83-01 (Tocris), 3 µM SB202190 (Cayman Chemicals) and 10 nM prostaglandin E2 (Cayman Chemicals). Organoids were passaged depending on growth every 1–2 weeks by incubating in TrypLE Express (Gibco) for 5–10 min followed by embedding in BME. Organoids were authenticated by SNP array or STR profile and regularly tested for Mycoplasma using Mycoplasma PCR43 and the MycoAlert Mycoplasma Detection Kit (cat no. LT07-318). In the first two weeks of organoid culture, 1x Primocin (Invivogen) was added to prevent microbial contamination. Procedures performed with patient specimens were approved by the Medical Ethical Committee of the Netherlands Cancer Institute – Antoni van Leeuwenhoek hospital (study NL48824.031.14) and written informed consent was obtained from all patients. Mismatch repair status was assessed by standard protocol for the Ventana automated immunostainer for MLH1 clone M1 (Roche), MSH2 clone G219-1129 (Roche), MSH6 clone EP49 (Abcam) and PMS2 clone EP51 (Agilant Technologies). The *B2M*^{KO} tumor organoid lines were generated by using sgRNA targeting *B2M* (GGCCGAGATGTCTCGCTCCG), cloned into LentiCRISPR v2 plasmid. The virus was produced by standard method.

Screening of cancer cell lines and tumor organoids by flow cytometry

The cancer cell lines used in the reactivity and killing assays were screened for the expression of β2m, HLA class I molecules, NKG2D ligands, DNAM-1 ligands, and butyrophilin by flow cytometry. Briefly, cells were incubated with human Fc receptor block (BioLegend) and stained with the different cell surface antibodies (1:10 anti-CD112-PE [clone R2.525, BD Biosciences], 1:10 anti-CD155-PE [clone 300907, R&D Systems], 1:50 anti-CD277/BTN3A1-PE [clone BT3.1, Miltenyi], 1:100 anti-β2M-PE [clone 2M2, BioLegend], 1:100 anti-HLA-A/B/C-FITC [clone W6/32, eBioscience], 1:160 anti-HLA-A/B/C-AF647 [clone W6/32, BioLegend], 1:20 anti-HLA-E-BV421 [clone 3D12, BioLegend], 1:20 anti-HLA-G-APC [clone 87G, BioLegend], 1:300 anti-MICA/B-PE [clone 6D4, BioLegend], 1:10 anti-ULBP1-PE [clone 170818, R&D Systems], 1:20 anti-ULBP2/5/6-PE [clone 165903, R&D Systems], 1:20 anti-ULBP3-PE [clone 166510, R&D Systems], or 1:20 anti-ULBP4-PE [clone 709116, R&D Systems] for 45 min at 4°C. A 1:1000 live/dead fixable near-infrared viability dye (Life Technologies) was included in each staining. Cells were washed three times in FACS buffer (PBS/1% FCS). Compensation was carried out with CompBeads (BD Biosciences) and ArC reactive beads (Life Technologies). Cells were acquired on a FACS Canto II 3L or FACS LSR Fortessa 4L (BD Biosciences) running FACSDiva software version 9.0 (BD Biosciences). Isotype or FMO controls were included to determine the percentage of positive cancer cells. Data were analyzed with FlowJo software version 10.6.1 (Tree Star Inc).

For organoid surface staining, tumor organoids were dissociated into single cells using TrypLE Express (Gibco) washed twice in cold FACS buffer (PBS, 5 mM EDTA, 1% bovine serum antigen) and stained with either 1:20 anti-HLA-A,B,C-PE (clone W6/32, BD Biosciences), 1:100 anti-β2m-FITC (clone 2M2, BioLegend), 1:200 anti-PD-L1 (clone MIH1, eBioscience) and 1:2000 near-infrared (NIR) viability dye (Life Technologies) or isotype controls (FITC, PE or APC) mouse IgG1 kappa (BD Biosciences). For NKG2D ligand expression analysis cells were stained with 1:300 anti-MICA/MICB, 1:10 anti-ULBP1, 1:20 anti-ULBP2/5/6, 1:20 anti-ULBP3, 1:20 anti-ULBP4, and 1:2000 near-infrared (NIR) viability dye (Life Technologies). Tumor cells were incubated for 30 min at 4°C in the dark and washed twice in FACS buffer. All samples were recorded at a Becton Dickinson Fortessa.

Reactivity assay γδ T cells

Reactivity of γδ T cells to the different cancer cell lines was assessed by a co-culture reactivity assay. γδ T cells were thawed and cultured in IMDM+Glutamax (Gibco)/8% nHS medium with pen (100 IU/mL)/strep (100 µg/mL) in the presence of low-dose IL-2 (25 IU/mL) and IL-15 (5 ng/mL) overnight at 37°C. Cancer cell lines were counted, adjusted to a concentration of $0.5x10^5$ cells/mL in IMDM+Glutamax/10% FCS medium with pen (100 IU/mL)/strep (100 µg/mL), and seeded (100 µL/well) in coated 96-well flat-bottom microplates (Greiner CellStar) (for 5,000 cells/well) overnight at 37°C. The next day, γδ T cells were harvested, counted, and adjusted to a concentration of $1.2x10^6$ cells/mL in IMDM+Glutamax/10% FCS medium. The γδ T cells were added in 50 µL (for 60,000 cells/well) and co-cultured (12:1 E:T ratio) at 37°C for 18h in biological triplicates. Medium (without cancer cells) was used as negative control and PMA (20 ng/mL)/ionomycin (1 µg/mL) as positive control. After co-culture, the supernatant was harvested to detect IFN-γ secretion by ELISA (Mabtech) following the manufacturer's instructions. Additionally, cells were harvested, incubated with human Fc receptor block (BioLegend), and stained with cell surface antibodies (1:100 anti-CD137-APC [clone 4B4-1, BD Biosciences], 1:150 anti-CD226/DNAM-1-BV510 [clone DX11, BD Biosciences], 1:400 anti-CD3-AF700 [clone UCHT1, BD Biosciences], 1:80 anti-CD39-APC [clone A1, BioLegend], 1:10 anti-CD40L-PE [clone TRAP1, BD Biosciences] or 1:30 anti-PD-1-PE [clone MIH4, eBioscience], 1:40 anti-TCRγδ-BV650 [clone 11F2, BD Biosciences], 1:300 anti-NKG2D-PE-Cy7 [clone 1D11, BD Biosciences], and 1:20 anti-OX40-FITC [clone ACT35, BioLegend] for 45 min at 4°C. A 1:1000 live/dead fixable near-infrared viability dye (Life Technologies) was included in each staining. Cells were washed three times in FACS buffer (PBS/1% FCS). Compensation was carried out with CompBeads (BD Biosciences) and ArC reactive beads (Life Technologies). Cells were acquired on a FACS LSR Fortessa X-20 4L (BD Biosciences) running FACSDiva software version 9.0 (BD Biosciences). Data were analyzed with FlowJo software version 10.6.1 (Tree Star Inc). All data are

representative of at least two independent experiments.

Immune cell killing assay γδ T cells

Killing of the different cancer cell lines by γδ T cells was visualized and quantified by a co-culture immune cell killing assay using the IncuCyte S3 Live-Cell Analysis System (Essen Bioscience). HCT-15, LoVo, and HT-29 cells were transduced with IncuCyte NucLight Red Lentivirus Reagent (EF-1α, Puro; Essen BioScience) providing a nuclear-restricted expression of a red (mKate2) fluorescent protein. In short, HCT-15, LoVo and HT-29 were seeded, transduced according to the manufacturer's instructions, and stable cell populations were generated using puromycin selection. The *B2M*-knockin cell lines were created under puromycin selection, hence, stable NucLight Red-expressing cell populations were generated by sorting mKate2 (the red fluorescent protein) in the PE Texas Red filter set instead. Cancer cell lines were counted, adjusted to a concentration of $1x10^5$ cells/mL in IMDM+Glutamax/10% FCS medium with pen (100 IU/mL)/strep (100 µg/mL), and seeded (100 µL/well) in 96-well flat-bottom clear microplates (Greiner CellStar) (for 10,000 cells/well). The target cell plate was placed in the IncuCyte system at 37°C to monitor for cell confluency for 3 days. On day 2, γδ T cells were thawed and cultured in IMDM+Glutamax/8% nHS medium with pen (100 IU/mL)/strep (100 µg/mL) in the presence of low-dose IL-2 (25 IU/mL) and IL-15 (5 ng/mL) overnight at 37°C. The next day, γδ T cells were harvested, counted, and adjusted to a concentration of $7.2x10^5$ cells/mL in IMDM+Glutamax/10% FCS medium. After aspiration of the medium of the target cell plate, 100 µL of new medium containing 3.75 µM IncuCyte Caspase-3/7 Green Apoptosis Reagent (Essen BioScience) (1.5x final assay concentration of 2.5 µM) was added together with 50 µL of γδ T cells (for 36,000 cells/well). They were co-cultured (4:1 E:T ratio) in the IncuCyte system at 37°C in biological duplicates. Cancer cells alone and cancer cells alone with Caspase-3/7 were used as negative controls. Images (2 images/well) were captured every hour at 20x magnification with the phase, green, and red channels for up to 4 days.

Analysis was performed in the IncuCyte software (version 2020B) for each cancer cell line separately. The following analysis definitions were applied: 1) for HCT-15 cells in the phase channel a minimum area of 200 μm^2, in the green channel a threshold of 2 GCU, and in the red channel a threshold of 2 RCU, 2) for LoVo and HT-29 cells in the phase channel a minimum area of 200 μm^2, in the green channel a threshold of 4 GCU, and in the red channel a threshold of 2 RCU. Cancer cell apoptosis was then quantified in the IncuCyte software by counting the total number of Green + Red objects per image normalized (by division) to the total number of Red objects per image after 12h co-culture and displayed as a percentage (mean ± SEM) of two wells with two images/well. For the comparison of the killing of *B2M*-knockin HCT-15 and LoVo cell lines *vs* the wildtype cell lines, Caspase-3/7 Red Apoptosis Reagent (Essen BioScience) was used. The transfection of the target reporter was not as successful in combination with the *B2M*-knockin. Hence, apoptosis was quantified by dividing the Red area by the Phase area and displayed as a percentage (mean ± SEM) of two wells with two images/well. The following analysis definitions were applied: a minimum phase area of 100 μm^2 and a RCU of 0.5 (for HCT-15) and 0.75 (for LoVo).

Tumor organoid recognition assay

For evaluation of tumor reactivity toward $B2M^{WT}$ and $B2M^{KO}$ organoids and NKG2D ligand blocking conditions, tumor organoids and γδ T cells were prepared as described previously.[9,66,67] Two days prior to the experiment organoids were isolated from BME by incubation in 2 mg/mL type II dispase (Sigma-Aldrich) for 15 min before addition of 5 mM ethylendiaminetetraacetic acid (EDTA) and washed with PBS before resuspended in CRC organoid medium with 10 µM Y-27632 (Sigma-Aldrich). Organoids were stimulated with 200 ng/mL IFN-γ (Peprotech) 24 hours before the experiment. For the recognition assay and intra-cellular staining tumor organoids were dissociated into single cells and plated in anti-CD28 (clone CD28.2 eBioscience) coated 96-well U-bottom plates with γδ T cells at a 1:1 target:effector ratio in the presence of 20 µg/mL anti-PD-1 (Merus). As positive control γδ T cells were stimulated with 50 ng/mL of phorbol 12-myristate 13 -acetate (Sigma-Aldrich) and 1 µg/mL of ionomycin (Sigma-Aldrich). After

1h of incubation at 37°C, GolgiSTOP (BD Biosciences, 1:1500) and GolgiPlug (BD Biosciences, 1:1000) were added. After 4h of incubation at 37°C, γδ T cells were washed twice in cold FACS buffer (PBS, 5 mM EDTA, 1% bovine serum antigen) and stained with 1:20 anti-CD3-PerCP-Cy5.5 (BD Biosciences), 1:20 anti-TCRγδ-PE (BD Bioscience), 1:20 anti-CD4-FITC (BD Bioscience) (not added in experiments with NKG2D ligand blocking), 1:200 anti-CD8-BV421 (BD Biosciences) and 1:2000 near-infrared (NIR) viability dye (Life Technologies) for 30 min at 4°C. Cells were washed, fixed and stained with 1:40 anti-IFN-γ-APC (BD Biosciences) for 30 min at 4°C, using the Cytofix/Cytoperm Kit (BD Biosciences). After two washing steps, cells were resuspended in FACS buffer and recorded at a BD LSRFortessa™ Cell Analyzer SORP flow cytometer with FACSDiVa 8.0.2 (BD Biosciences) software.

Blocking experiments with cancer cell lines and tumor organoids

Reactivity of and killing by the γδ T cells was examined in the presence of different blocking antibodies to investigate which receptor-ligand interactions are involved. For DNAM-1 blocking, γδ T cells were incubated with 3 µg/mL purified anti-DNAM-1 (clone DX11, BD Biosciences) for 1h at 37°C. For γδ TCR blocking, γδ T cells were incubated with 3 µg/mL purified anti-TCRγδ (clone 5A6.E9, Invitrogen) for 1h at 37°C, of which the clone we used was tested to be best for use in γδ TCR blocking assays[68]. NKG2D ligands were blocked on the cancer cell lines and single cells of tumor organoids by incubating the target cells with 12 µg/mL anti-MICA/B (clone 6D4, BioLegend), 1 µg/mL anti-ULBP1 (clone 170818, R&D Systems), 3 µg/mL anti-ULBP2/5/6 (clone 165903, R&D Systems), and 6 µg/mL anti-ULBP3 (clone 166510, R&D Systems) for 1h at 37°C prior to plating with γδ T cells. After incubation with the blocking antibodies, the γδ T cells were added to cancer cell lines HCT-15, LoVo, and HT-29 as described above with a minimum of two biological replicates per blocking condition. For organoid experiments, 1:50 anti-CD107a-FITC (clone H4A3, BioLegend) was added during incubation.

As a control for Fc-mediated antibody effector functions, γδ T cells alone were incubated with the blocking antibodies in the presence of 2.5 µM IncuCyte Caspase-3/7 Green Apoptosis Reagent (Essen BioScience) in the IncuCyte system at 37°C, and the number of apoptotic γδ T cells was quantified over time.

Data availability

The used TCGA data is publicly available via the National Cancer Institute GDC Data Portal (https://portal.gdc.cancer.gov; cohorts COAD, STAD and UCEC). Of DRUP study subjects included in this preliminary analysis across all (complete and incomplete) cohorts of the study, we included all clinical data, genomics data on *B2M* status and RNA-expression data of marker gene sets to this manuscript in **Table S1**. As mentioned in the original publication, NICHE study RNA- and DNA-sequencing data is deposited into the European Genome–Phenome Archive under accession no. EGAS00001004160 and will be made available on reasonable request for academic use and within the limitations of the provided informed consent. The single-cell RNA-sequencing data are available from the corresponding author upon request. All other data are available from the corresponding author upon reasonable request.

ACKNOWLEDGEMENTS

We thank K.C.M.J. Peeters, M.G. Kallenberg-Lantrua, D. Berends-van der Meer, and F.A. Holman for their help in collecting and providing samples from patients with colon cancer; the Flow cytometry Core Facility of the Leiden University Medical Center for their help with cell sorting; the Leiden Genome Technology Center for their help with single-cell RNA-sequencing; and M. Ganesh for help with cell culturing. We thank D. Thommen for fruitful discussions, I. S. Rodriguez for the establishment of a *B2M*-knockout organoid line, L. Hoes for initial clinical findings, the Flow Cytometry Core Facility at the Netherlands Cancer Institute for their support; X. Kong for providing the lentiCRISPR plasmid for *B2M*-knockout; Merus for providing anti-PD-1 for organoid experiments; The Cancer Genome Atlas (TCGA) for providing data used in this manuscript.

AUTHOR CONTRIBUTIONS

N.L.d.V., J.v.d.H. and V.V. conceived the study and performed experiments. J.v.d.H. performed bulk transcriptomic analyses of ICB-naïve as well as ICB-treated MMR-d cancers. N.L.d.V. performed single-cell RNA-sequencing and cell culturing experiments. V.V. performed organoid experiments. N.L.d.V., M.v.d.P. and J.v.d.B. performed cell line and IncuCyte experiments. N.L.d.V., V.V. and M.v.d.P. performed blocking experiments. M.C. provided tissue sections of patients in the NICHE study, which was designed and coordinated by M.C. under joint supervision of T.N.S., E.E.V. and J.B.H. M.E.I. carried out imaging mass cytometry experiments. M.E.I., N.F.C.C.d.M., N.L.d.V. and D.R. analyzed the imaging mass cytometry data. N.L.d.V. and D.R. analyzed the single-cell RNA-sequencing data. J.G.v.d.B. evaluated histological and immunohistochemical analyses. L.J.Z., B.S.G., G.F.d.W., T.W.B., H.G. and H.M.W.V. designed, coordinated, and analyzed data from the DRUP study. General scientific coordination by J.v.d.H. L.F.A.W., F.K., N.F.C.C.d.M. and E.E.V. supervised the study, with an advisory role of T.N.S. The manuscript was written by N.L.d.V., J.v.d.H. and V.V. in collaboration with all co-authors. All authors commented on and approved the manuscript.

COMPETING INTERESTS

The authors have no competing interests to declare.

REFERENCES

1 Ionov, Y., Peinado, M. A., Malkhosyan, S., Shibata, D. & Perucho, M. Ubiquitous somatic mutations in simple repeated sequences reveal a new mechanism for colonic carcinogenesis. *Nature* 363, 558-561, doi:10.1038/363558a0 (1993).

2 Germano, G. *et al.* Inactivation of DNA repair triggers neoantigen generation and impairs tumour growth. *Nature* 552, 116-120, doi:10.1038/nature24673 (2017).

3 Zaretsky, J. M. *et al.* Mutations Associated with Acquired Resistance to PD-1 Blockade in Melanoma. *N Engl J Med* 375, 819-829, doi:10.1056/NEJMoa1604958 (2016).

4 Gettinger, S. *et al.* Impaired HLA Class I Antigen Processing and Presentation as a Mechanism of Acquired Resistance to Immune Checkpoint Inhibitors in Lung Cancer. *Cancer Discov* 7, 1420-1435, doi:10.1158/2159-8290.Cd-17-0593 (2017).

5 Sade-Feldman, M. *et al.* Resistance to checkpoint blockade therapy through inactivation of antigen presentation. *Nat Commun* 8, 1136, doi:10.1038/s41467-017-01062-w (2017).

6 Le, D. T. *et al.* Mismatch repair deficiency predicts response of solid tumors to PD-1 blockade. *Science* 357, 409-413, doi:10.1126/science.aan6733 (2017).

7 Overman, M. J. *et al.* Nivolumab in patients with metastatic DNA mismatch repair-deficient or microsatellite instability-high colorectal cancer (CheckMate 142): an open-label, multicentre, phase 2 study. *The Lancet. Oncology* 18, 1182-1191, doi:10.1016/s1470-2045(17)30422-9 (2017).

8 Overman, M. J. *et al.* Durable Clinical Benefit With Nivolumab Plus Ipilimumab in DNA Mismatch Repair-Deficient/Microsatellite Instability-High Metastatic Colorectal Cancer. *Journal of clinical oncology : official journal of the American Society of Clinical Oncology* 36, 773-779, doi:10.1200/jco.2017.76.9901 (2018).

9 Chalabi, M. *et al.* Neoadjuvant immunotherapy leads to pathological responses in MMR-proficient and MMR-deficient early-stage colon cancers. *Nat Med* 26, 566-576, doi:10.1038/s41591-020-0805-8 (2020).

10 Dolcetti, R. *et al.* High prevalence of activated intraepithelial cytotoxic T lymphocytes and increased neoplastic cell apoptosis in colorectal carcinomas with microsatellite instability. *Am J Pathol* 154, 1805-1813, doi:10.1016/s0002-9440(10)65436-3 (1999).

11 Tumeh, P. C. *et al.* PD-1 blockade induces responses by inhibiting adaptive immune resistance. *Nature* 515, 568-571, doi:10.1038/nature13954 (2014).

12 Taube, J. M. *et al.* Association of PD-1, PD-1 ligands, and other features of the tumor immune microenvironment with response to anti-PD-1 therapy. *Clin Cancer Res* 20, 5064-5074, doi:10.1158/1078-0432.Ccr-13-3271 (2014).

13 Bicknell, D. C., Kaklamanis, L., Hampson, R., Bodmer, W. F. & Karran, P. Selection for beta 2-microglobulin mutation in mismatch repair-defective colorectal carcinomas. *Current biology : CB* 6, 1695-1697, doi:10.1016/s0960-9822(02)70795-1 (1996).

14 Kloor, M. *et al.* Immunoselective pressure and human leukocyte antigen class I antigen machinery defects in microsatellite unstable colorectal cancers. *Cancer Res* 65, 6418-6424, doi:10.1158/0008-5472.can-05-0044 (2005).

15 Dierssen, J. W. *et al.* HNPCC versus sporadic microsatellite-unstable colon cancers follow different routes toward loss of HLA class I expression. *BMC Cancer* 7, 33, doi:10.1186/1471-2407-7-33 (2007).

16 Ijsselsteijn, M. E. *et al.* Revisiting immune escape in colorectal cancer in the era of immunotherapy. *Br J Cancer* 120, 815-818, doi:10.1038/s41416-019-0421-x (2019).

17 Hughes, E. A., Hammond, C. & Cresswell, P. Misfolded major histocompatibility complex class I heavy chains are translocated into the cytoplasm and degraded by the proteasome. *Proc Natl Acad Sci U S A* 94, 1896-1901, doi:10.1073/pnas.94.5.1896 (1997).

18 Middha, S. *et al.* Majority of B2M-Mutant and -Deficient Colorectal Carcinomas Achieve Clinical Benefit From Immune Checkpoint Inhibitor Therapy and Are Microsatellite Instability-High. *JCO precision oncology* 3, doi:10.1200/po.18.00321 (2019).

19 Groh, V. *et al.* Human lymphocytes bearing T cell receptor gamma/delta are phenotypically diverse and evenly distributed throughout the lymphoid system. *J Exp Med* 169, 1277-1294, doi:10.1084/jem.169.4.1277 (1989).

20 Silva-Santos, B., Serre, K. & Norell, H. γδ T cells in cancer. *Nat Rev Immunol* 15, 683-691, doi:10.1038/nri3904 (2015).

21 Halary, F. *et al.* Control of self-reactive cytotoxic T lymphocytes expressing gamma delta T cell receptors by natural killer inhibitory receptors. *Eur J Immunol* 27, 2812-2821, doi:10.1002/eji.1830271111 (1997).

22 de Vries, N. L. *et al.* High-dimensional cytometric analysis of colorectal cancer reveals novel mediators of antitumour immunity. *Gut* 69, 691-703, doi:10.1136/gutjnl-2019-318672 (2020).

23 van der Velden, D. L. *et al.* The Drug Rediscovery protocol facilitates the expanded use of existing anticancer drugs. *Nature* 574, 127-131, doi:10.1038/s41586-019-1600-x (2019).

24 Danaher, P. *et al.* Gene expression markers of Tumor Infiltrating Leukocytes. *J Immunother Cancer* 5, 18, doi:10.1186/s40425-017-0215-8 (2017).

25 Duhen, T. *et al.* Co-expression of CD39 and CD103 identifies tumor-reactive CD8 T cells in human solid tumors. *Nat Commun* 9, 2724, doi:10.1038/s41467-018-05072-0 (2018).

26 Kwon, M. *et al.* Determinants of Response and Intrinsic Resistance to PD-1 Blockade in Microsatellite Instability-High Gastric Cancer. *Cancer Discov*, doi:10.1158/2159-8290.Cd-21-0219 (2021).

27 Wu, P. *et al.* γδT17 cells promote the accumulation and expansion of myeloid-derived suppressor cells in human colorectal cancer. *Immunity* 40, 785-800, doi:10.1016/j.immuni.2014.03.013 (2014).

28 Lo Presti, E., Dieli, F. & Meraviglia, S. Tumor-Infiltrating γδ T Lymphocytes: Pathogenic Role, Clinical Significance, and Differential Programing in the Tumor Microenvironment. *Front Immunol* 5, 607, doi:10.3389/fimmu.2014.00607 (2014).

29 Maeurer, M. J. *et al.* Human intestinal Vdelta1+ lymphocytes recognize tumor cells of epithelial origin. *J Exp Med* 183, 1681-1696, doi:10.1084/jem.183.4.1681 (1996).

30 Siegers, G. M., Ribot, E. J., Keating, A. & Foster, P. J. Extensive expansion of primary human gamma delta T cells generates cytotoxic effector memory cells that can be labeled with Feraheme for cellular MRI. *Cancer Immunol Immunother* 62, 571-583, doi:10.1007/s00262-012-1353-y (2013).

31 Wu, D. *et al.* Ex vivo expanded human circulating Vδ1 γδT cells exhibit favorable therapeutic potential for colon cancer. *Oncoimmunology* 4, e992749, doi:10.4161/2162402x.2014.992749 (2015).

32 Almeida, A. R. *et al.* Delta One T Cells for Immunotherapy of Chronic Lymphocytic Leukemia: Clinical-Grade Expansion/Differentiation and Preclinical Proof of Concept. *Clin Cancer Res* 22, 5795-5804, doi:10.1158/1078-0432.Ccr-16-0597 (2016).

33 Mikulak, J. *et al.* NKp46-expressing human gut-resident intraepithelial Vδ1 T cell subpopulation exhibits high antitumor activity against colorectal cancer. *JCI insight* 4, doi:10.1172/jci.insight.125884 (2019).

34 van der Leun, A. M., Thommen, D. S. & Schumacher, T. N. CD8(+) T cell states in human cancer: insights from single-cell analysis. *Nat Rev Cancer* 20, 218-232, doi:10.1038/s41568-019-0235-4 (2020).

35 Groh, V., Steinle, A., Bauer, S. & Spies, T. Recognition of stress-induced MHC molecules by intestinal epithelial gammadelta T cells. *Science* 279, 1737-1740, doi:10.1126/science.279.5357.1737 (1998).

36 Groh, V. *et al.* Broad tumor-associated expression and recognition by tumor-derived gamma delta T cells of MICA and MICB. *Proc Natl Acad Sci U S A* 96, 6879-6884, doi:10.1073/pnas.96.12.6879 (1999).

37 Poggi, A. *et al.* Vdelta1 T lymphocytes from B-CLL patients recognize ULBP3 expressed on leukemic B cells and up-regulated by trans-retinoic acid. *Cancer Res* 64, 9172-9179, doi:10.1158/0008-5472.Can-04-2417 (2004).

38 Hause, R. J., Pritchard, C. C., Shendure, J. & Salipante, S. J. Classification and characterization of microsatellite instability across 18 cancer types. *Nat Med* 22, 1342-1350, doi:10.1038/nm.4191 (2016).

39 Cader, F. Z. *et al.* A peripheral immune signature of responsiveness to PD-1 blockade in patients with classical Hodgkin lymphoma. *Nat Med* 26, 1468-1479, doi:10.1038/s41591-020-1006-1 (2020).

40 Germano, G. *et al.* CD4 T cell dependent rejection of beta 2 microglobulin null mismatch repair deficient tumors. *Cancer Discov*, doi:10.1158/2159-8290.Cd-20-0987 (2021).

41 Carter, S. L. *et al.* Absolute quantification of somatic DNA alterations in human cancer. *Nat Biotechnol* 30, 413-421, doi:10.1038/nbt.2203 (2012).

42 Taylor, A. M. *et al.* Genomic and Functional Approaches to Understanding Cancer Aneuploidy. *Cancer Cell* 33, 676-689 e673, doi:10.1016/j.ccell.2018.03.007 (2018).

43 Thorsson, V. *et al.* The Immune Landscape of Cancer. *Immunity* 51, 411-412, doi:10.1016/j.immuni.2019.08.004 (2019).

44 Priestley, P. *et al.* Pan-cancer whole-genome analyses of metastatic solid tumours. *Nature* 575, 210-216, doi:10.1038/s41586-019-1689-y (2019).

45 Huang, M. N. *et al.* MSIseq: Software for Assessing Microsatellite Instability from Catalogs of Somatic Mutations. *Sci Rep* 5, 13321, doi:10.1038/srep13321 (2015).

46 Dobin, A. *et al.* STAR: ultrafast universal RNA-seq aligner. *Bioinformatics (Oxford, England)* 29, 15-21, doi:10.1093/bioinformatics/bts635 (2013).

47 Cameron, D. L. *et al.* GRIDSS, PURPLE, LINX: Unscrambling the tumor genome via integrated analysis of structural variation and copy number. *bioRxiv*, 781013, doi:10.1101/781013 (2019).

48 Robinson, J. T. *et al.* Integrative genomics viewer. *Nat Biotechnol* 29, 24-26, doi:10.1038/nbt.1754 (2011).

49 Virtanen, P. *et al.* SciPy 1.0: fundamental

algorithms for scientific computing in Python. *Nat Methods* 17, 261-272, doi:10.1038/s41592-019-0686-2 (2020).

50 Robinson, M. D., McCarthy, D. J. & Smyth, G. K. edgeR: a Bioconductor package for differential expression analysis of digital gene expression data. *Bioinformatics (Oxford, England)* 26, 139-140, doi:10.1093/bioinformatics/btp616 (2010).

51 Ritchie, M. E. *et al.* limma powers differential expression analyses for RNA-sequencing and microarray studies. *Nucleic Acids Res* 43, e47, doi:10.1093/nar/gkv007 (2015).

52 Law, C. W., Chen, Y., Shi, W. & Smyth, G. K. voom: Precision weights unlock linear model analysis tools for RNA-seq read counts. *Genome Biol* 15, R29, doi:10.1186/gb-2014-15-2-r29 (2014).

53 Hall, G. *et al.* Immunohistochemistry for PMS2 and MSH6 alone can replace a four antibody panel for mismatch repair deficiency screening in colorectal adenocarcinoma. *Pathology* 42, 409-413, doi:10.3109/00313025.2010.493871 (2010).

54 Stoeckius, M. *et al.* Simultaneous epitope and transcriptome measurement in single cells. *Nat Methods* 14, 865-868, doi:10.1038/nmeth.4380 (2017).

55 Stuart, T. *et al.* Comprehensive Integration of Single-Cell Data. *Cell* 177, 1888-1902 e1821, doi:10.1016/j.cell.2019.05.031 (2019).

56 McGinnis, C. S. *et al.* MULTI-seq: sample multiplexing for single-cell RNA sequencing using lipid-tagged indices. *Nat Methods* 16, 619-626, doi:10.1038/s41592-019-0433-8 (2019).

57 Haghverdi, L., Lun, A. T. L., Morgan, M. D. & Marioni, J. C. Batch effects in single-cell RNA-sequencing data are corrected by matching mutual nearest neighbors. *Nat Biotechnol* 36, 421-427, doi:10.1038/nbt.4091 (2018).

58 McInnes, L., Healy, J. & Melville, J. J. a. p. a. Umap: Uniform manifold approximation and projection for dimension reduction. (2018).

59 Ijsselsteijn, M. E., van der Breggen, R., Farina Sarasqueta, A., Koning, F. & de Miranda, N. F. C. C. A 40-Marker Panel for High Dimensional Characterization of Cancer Immune Microenvironments by Imaging Mass Cytometry. *Frontiers in immunology* 10, 2534-2534, doi:10.3389/fimmu.2019.02534 (2019).

60 Berg, S. *et al.* ilastik: interactive machine learning for (bio)image analysis. *Nat Methods* 16, 1226-1232, doi:10.1038/s41592-019-0582-9 (2019).

61 Ijsselsteijn, M. E., Somarakis, A., Lelieveldt, B. P. F., Höllt, T. & de Miranda, N. Semi-automated background removal limits data loss and normalises imaging mass cytometry data. *Cytometry A*, doi:10.1002/cyto.a.24480 (2021).

62 Carpenter, A. E. *et al.* CellProfiler: image analysis software for identifying and quantifying cell phenotypes. *Genome Biol* 7, R100, doi:10.1186/gb-2006-7-10-r100 (2006).

63 Somarakis, A., Van Unen, V., Koning, F., Lelieveldt, B. P. F. & Hollt, T. ImaCytE: Visual Exploration of Cellular Microenvironments for Imaging Mass Cytometry Data. *IEEE transactions on visualization and computer graphics*, 10.1109/TVCG.2019.2931299, doi:10.1109/TVCG.2019.2931299 (2019).

64 van der Maaten, L. J. P. & Hinton, G. E. Visualizing high-dimensional data using t-SNE. *J. Mach. Learn. Res.* 9, 2579-2605 (2008).

65 Höllt, T. *et al.* Cytosplore: Interactive Immune Cell Phenotyping for Large Single-Cell Datasets. 35, 171-180, doi:https://doi.org/10.1111/cgf.12893 (2016).

66 Dijkstra, K. K. *et al.* Generation of Tumor-Reactive T Cells by Co-culture of Peripheral Blood Lymphocytes and Tumor Organoids. *Cell* 174, 1586-1598.e1512, doi:10.1016/j.cell.2018.07.009 (2018).

67 Cattaneo, C. M. *et al.* Tumor organoid-T-cell coculture systems. *Nat Protoc* 15, 15-39, doi:10.1038/s41596-019-0232-9 (2020).

68 Dutta, I., Postovit, L. M. & Siegers, G. M. Apoptosis Induced via Gamma Delta T Cell Antigen Receptor "Blocking" Antibodies: A Cautionary Tale. *Front Immunol* 8, 776, doi:10.3389/fimmu.2017.00776 (2017).

SUPPLEMENTAL FIGURES

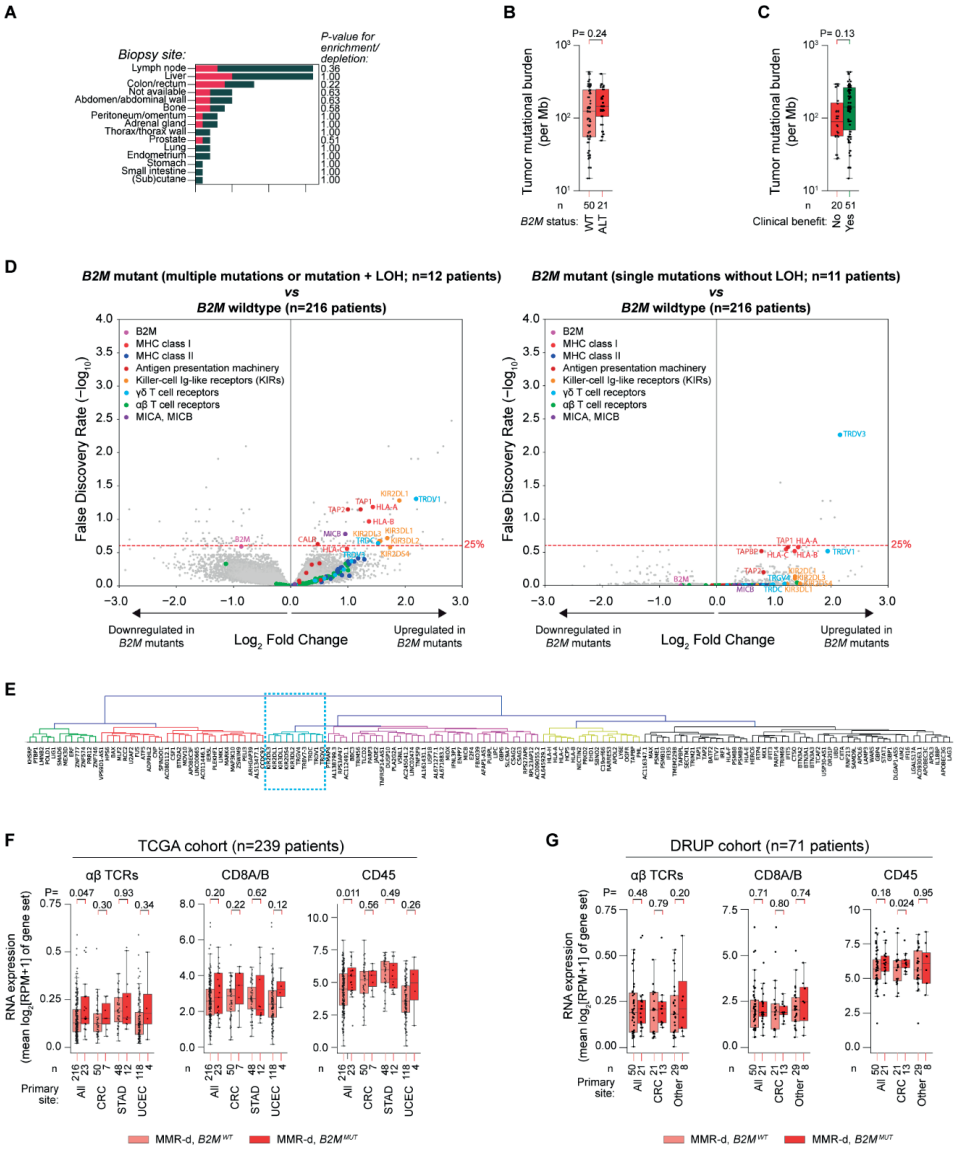

Figure S1. Association of *B2M* status to clinical, genomic, and transcriptomic characteristics of MMR-d tumors.

A. The number of patients per biopsy location for 71 patients in the DRUP with MMR-d cancers and available outcome of ICB therapy. Colors denote patients' *B2M* status (WT: wildtype, gray; ALT: altered, red). Fisher's exact test-based P-values for enrichment/depletion of *B2M* altered cases per primary site are shown. **B**. The tumor mutational burden per Mb *vs B2M* status. Wilcoxon rank sum test-based P-value is shown. **C.** The tumor mutational burden per Mb *vs* clinical benefit of immune checkpoint blockade (ICB). Wilcoxon rank sum test-based P-value is shown. **D.** Two volcano plots indicating differential gene expression between MMR-d cancers with wildtype *B2M vs* MMR-d cancers with multiple *B2M* mutations and/or *B2M* mutations + loss of heterozygosity (LOH; left plot), or *vs* MMR-d cancers with single *B2M* mutations without LOH (right plot). The Benjamini Hochberg false discovery rate (FDR) significance

threshold of 25% is indicated by the red dashed line. Results were obtained in a combined analysis of all MMR-d cancers of the TCGA COAD (colon adenocarcinoma; n=57 patients), STAD (stomach adenocarcinoma; n=60 patients) and UCEC (uterus corpus endometrial carcinoma; n=122 patients) cohorts, and were adjusted for tumor type. **E.** Dendrogram representing the hierarchical clustering result of gene expression profiles across all MMR-d cancers in the TCGA COAD (n=57 patients), STAD (n=60 patients) and UCEC (n=122 patients) cohorts. The genes included are those significantly (FDR <25%) upregulated in MMR-d *B2M*^{MUT} *vs* MMR-d *B2M*^{WT} cancers, after adjustment for tumor type. The blue dashed rectangle denotes the Vd1/3 T cell cluster. **F.** The RNA expression of different immune marker gene sets MMR-d *B2M*^{WT} (pink), and MMR-d *B2M*^{MUT} (red) cancers. Results are obtained with the TCGA COAD, STAD and UCEC cohorts, and are shown for all cohorts combined (All), and for each cohort separately. Boxes, whiskers, and dots indicate quartiles, 1.5 interquartile ranges, and individual data points, respectively. Wilcoxon rank sum test-based P-values are shown for MMR-d *B2M*^{WT} *vs* MMR-d *B2M*^{MUT} cancers. **G.** As **F**, but for MMR-d cancers in the DRUP cohort. Results are shown for all cancers combined (All), only colorectal cancer (CRC), or all non-CRC cancers (Other).

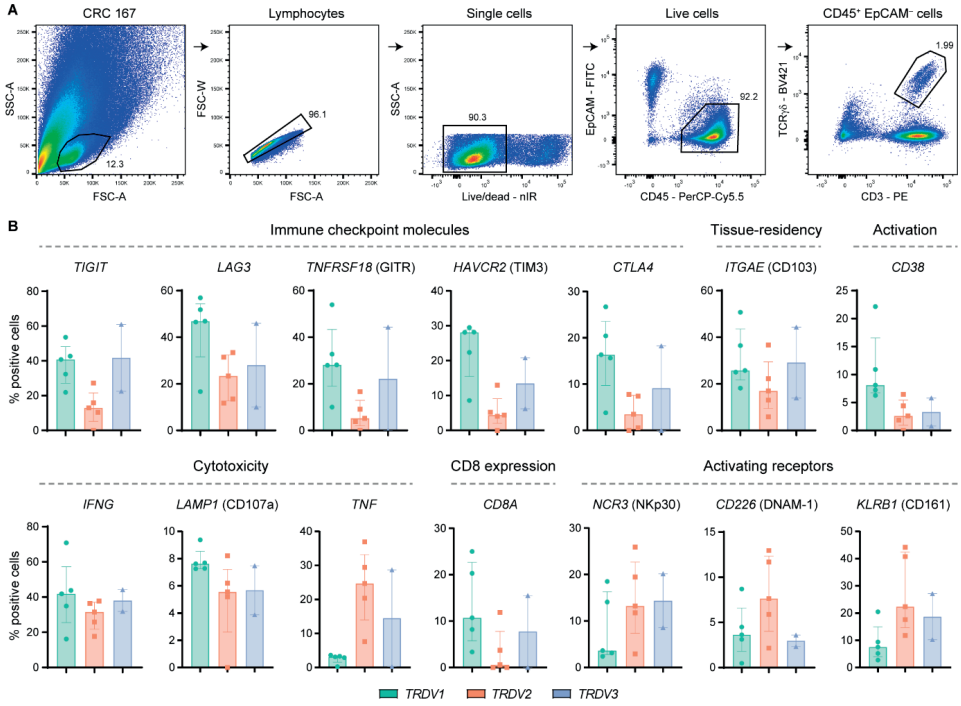

Figure S2. Characterization of γδ T cells from MMR-d colon cancers by single-cell RNA-sequencing.
A. FACS gating strategy for single, live CD45⁺ EpCAM⁻ CD3⁺ TCRγδ⁺ cells of a representative MMR-d colon cancer sample showing sequential gates with percentages. **B**. Frequencies of positive cells for selected genes across Vδ1 (n=1927), Vδ2 (n=860), and Vδ3 (n=506) cells as percentage of total γδ T cells from each MMR-d colon tumor (n=5) analyzed by single-cell RNA-sequencing. Vδ3 cells were present in two out of five colon cancers. Bars indicate median ± IQR. Each dot represents an individual sample.

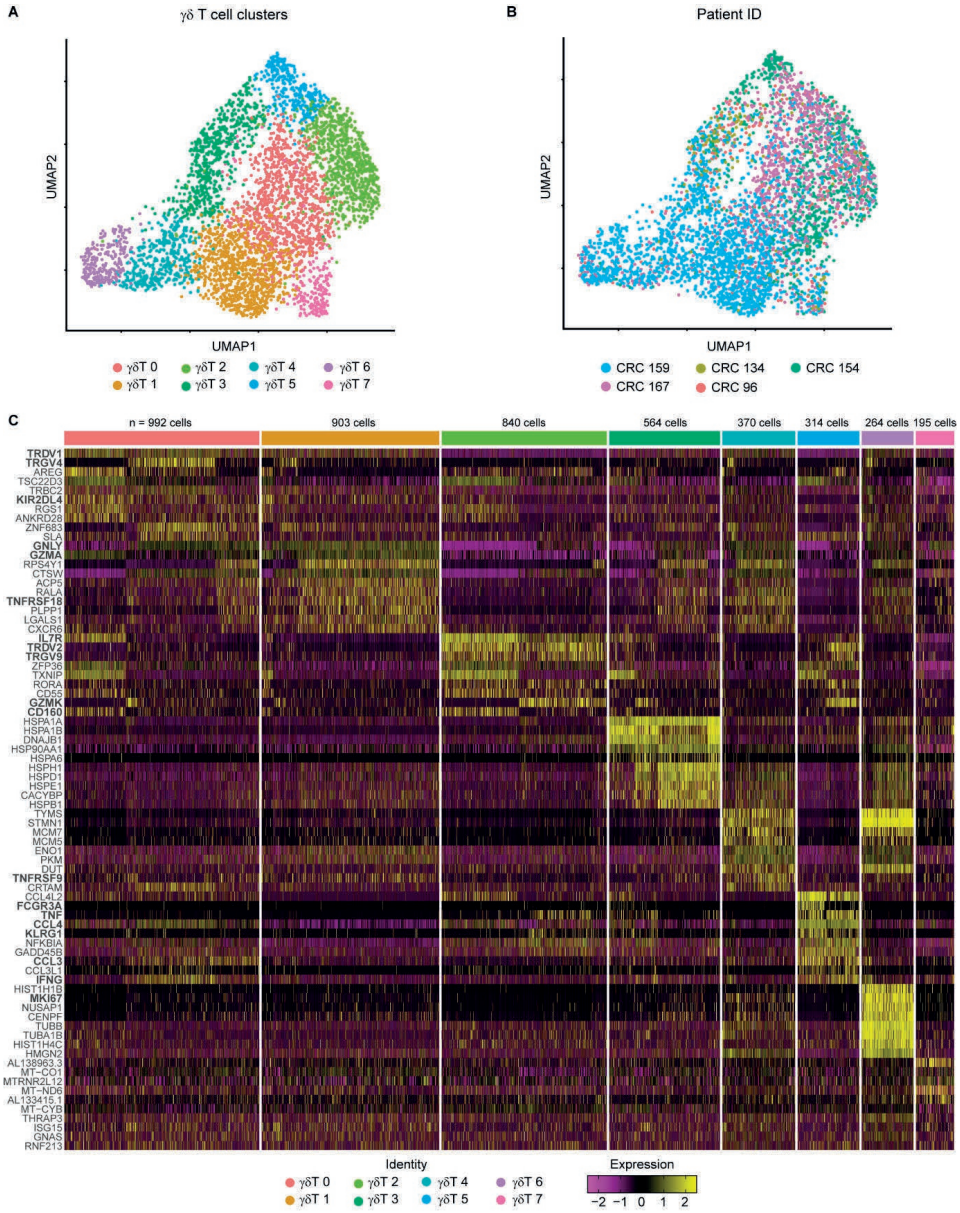

Figure S3. Distinct clusters of γδ T cells from MMR-d colon cancers by single-cell RNA-sequencing.
A. UMAP embedding showing γδ T cells (n=4442) isolated from MMR-d colon cancers (n=5) analyzed by single-cell RNA-sequencing. Colors represent the functionally different γδ T cell clusters identified by graph-based clustering and non-linear dimensional reduction. Each dot represents a single cell. **B**. UMAP embedding of (**A**) colored by patient ID. Each dot represents a single cell. **C**. Heatmap showing the normalized single-cell gene expression value (z-score, purple-to-yellow scale) for the top 10 differentially expressed genes in each identified γδ T cell cluster.

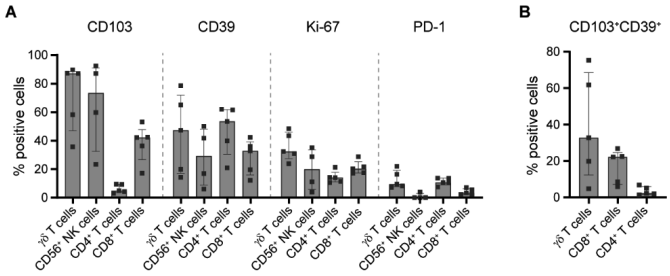

Figure S4. Phenotype of immune cell populations in β2m-positive and -negative MMR-d colon cancers.
A. Frequencies of marker-positive γδ T cells, $CD56^+$ NK cells, $CD4^+$ T cells, and $CD8^+$ T cells in treatment-naïve $\beta2m^-$ (n=5) MMR-d colon cancers. $CD56^+$ NK cells were present in four out of five $\beta2m^-$ cancer samples. Bars indicate median ± IQR. Each dot represents an individual sample. **B.** Frequencies of $CD103^+CD39^+$ γδ T cells, $CD8^+$ T cells, and $CD4^+$ T cells in treatment-naïve $\beta2m^-$ (n=5) MMR-d colon cancers. Bars indicate median ± IQR. Each dot represents an individual sample.

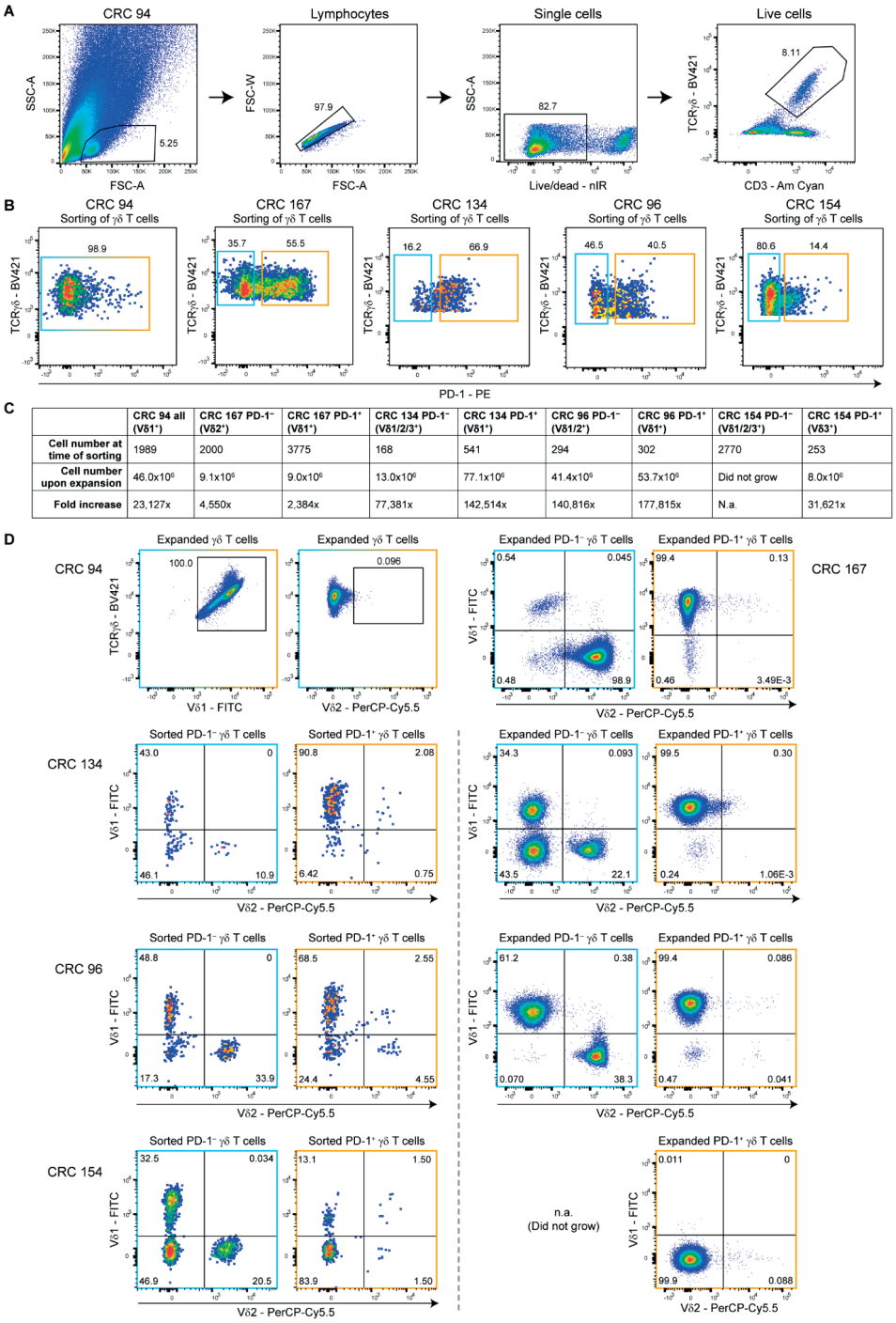

	CRC 94 all (Vδ1⁺)	CRC 167 PD-1⁻ (Vδ2⁺)	CRC 167 PD-1⁺ (Vδ1⁺)	CRC 134 PD-1⁻ (Vδ1/2/3⁺)	CRC 134 PD-1⁺ (Vδ1⁺)	CRC 96 PD-1⁻ (Vδ1/2⁺)	CRC 96 PD-1⁺ (Vδ1⁺)	CRC 154 PD-1⁻ (Vδ1/2/3⁺)	CRC 154 PD-1⁺ (Vδ3⁺)
Cell number at time of sorting	1989	2000	3775	168	541	294	302	2770	253
Cell number upon expansion	46.0x10⁶	9.1x10⁶	9.0x10⁶	13.0x10⁶	77.1x10⁶	41.4x10⁶	53.7x10⁶	Did not grow	8.0x10⁶
Fold increase	23,127x	4,550x	2,384x	77,381x	142,514x	140,816x	177,815x	N.a.	31,621x

Figure S5. Sorting of PD-1⁺ and PD-1⁻ γδ T cells from MMR-d colon cancers by FACS and their TCR Vδ chain usage.

A. FACS gating strategy for single, live CD3⁺ TCRγδ⁺ cells of a representative MMR-d colon cancer sample showing

sequential gates with percentages. **B**. Sorting of all γδ T cells from CRC94 (due to the low number of PD-1⁺ cells), and of PD-1⁻ (blue squares) and PD-1⁺ (orange squares) γδ T cells from CRC167, CRC134, CRC96, and CRC154. Each dot is a single cell. **C**. Table showing the number of γδ T cells isolated from colon cancers at the time of sorting *versus* 3-4 weeks after expansion, and the fold increase thereof. **D**. TCR Vδ chain usage after expansion of γδ T cells from CRC94 and CRC167 (first row), and at the time of sorting (left panel) as well as after expansion (right panel) of γδ T cells from CRC134, CRC96 and CRC154. From CRC154, the PD-1⁻ γδ T cells did not expand in culture. Each dot is a single cell.

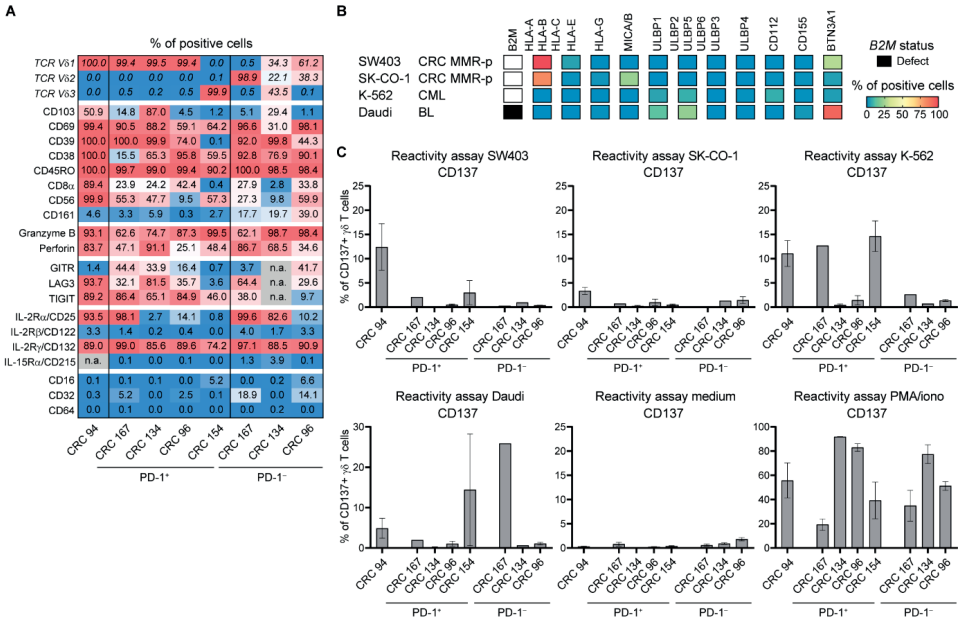

Figure S6. Phenotype and reactivity of γδ T cells from MMR-d colon cancers towards cancer cell lines.
A. Table showing the percentage of positive cells for different TCR Vδ chains (as in **Figure 3A**), tissue-residency/activation markers, cytotoxic molecules, immune checkpoint molecules, cytokine receptors, and Fc receptors on expanded PD-1⁺ and PD-1⁻ γδ T cells from MMR-d colon cancers (n=5) as percentage of total γδ T cells. **B**. Heatmap showing the *B2M* mutational status and surface expression of HLA class I, NKG2D ligands, DNAM-1 ligands, and butyrophilin on SW403, SK-CO-1, K-562, and Daudi cells. **C**. Bar plots showing the percentage of CD137-positive γδ T cells after 18h co-culture of PD-1⁺ and PD-1⁻ γδ T cells from MMR-d colon cancers (n=5) with SW403, SK-CO-1, K-562, and Daudi cells. Medium was used as negative control and PMA/ionomycin as positive control. Bars indicate mean ± SEM. Data from two independent experiments (CRC94, CRC134, CRC154, CRC96), depending on availability of γδ T cells.

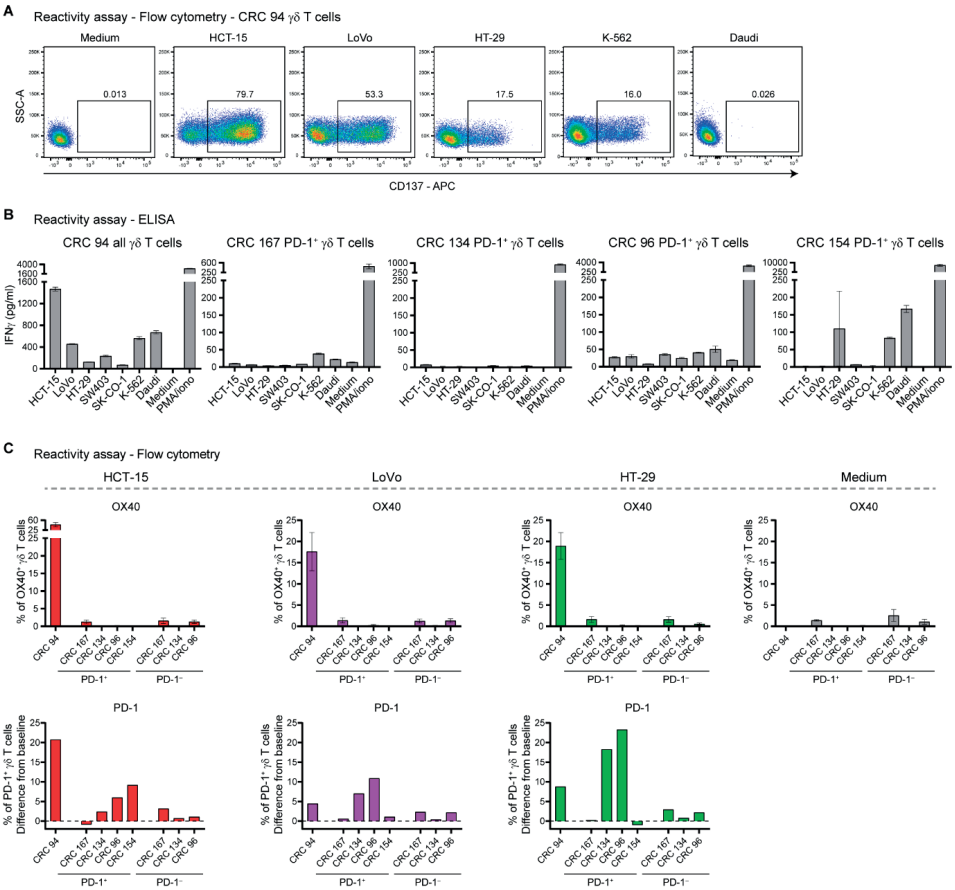

Figure S7. Reactivity of γδ T cells from MMR-d colon cancers towards cancer cell lines.
A. Representative flow cytometry plots showing the expression of CD137 on γδ T cells from CRC94 after 18h co-culture with HCT-15, LoVo, HT-29, K-562, and Daudi cells as compared to medium only. Gates indicate percentage of positive γδ T cells. **B**. Bar plots showing the presence of IFNg in the supernatant after 18h co-culture of PD-1$^+$ γδ T cells with the cancer cell lines. Medium as negative control and PMA/ionomycin as positive control are included. Bars indicate mean ± SEM of triplicates. **C**. Bar plots showing the percentage of OX40-positive (first row) and PD-1-positive (second row) γδ T cells after 18h co-culture of PD-1$^+$ and PD-1$^-$ γδ T cells from MMR-d colon cancers (n=5) with HCT-15, LoVo, and HT-29 cells. PD-1 expression is shown as difference from baseline (medium) condition. Bars indicate mean ± SEM. Data from four (CRC94), three (CRC167, CRC96), or two (CRC134, CRC154) independent experiments for OX40, depending on availability of γδ T cells.

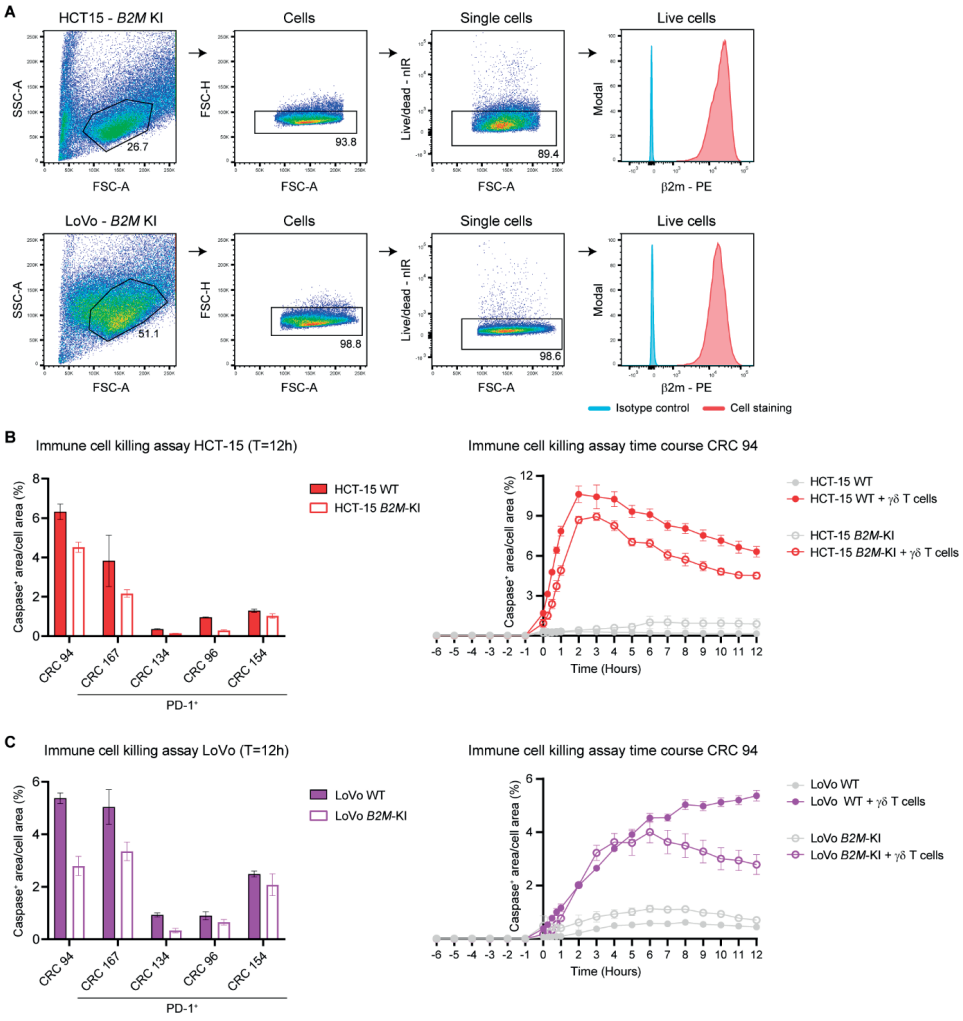

Figure S8. Characterization of *B2M*-knockin cancer cell lines and reactivity of γδ T cells towards *B2M*-knockin vs -wildtype cancer cell lines.

A. Flow cytometry gating strategy to validate β2m expression on HCT-15 and LoVo *B2M*-knockin (*B2M*-KI) cell lines. Isotype controls were included as negative control. **B**. Bar plots showing the quantification of the killing of HCT-15 *B2M*-KI *vs* wildtype (WT) cells by γδ T cells from MMR-d colon cancers (n=5) in the presence of a red fluorescent caspase-3/7 reagent after 12h co-culture. Bars indicate mean ± SEM of two wells with two images/well. Right panel shows representative time course of apoptosis (caspase-3/7) in the presence or absence of γδ T cells derived from CRC94. **C**. As **B**, but for LoVo *B2M*-KI *vs* WT cells.

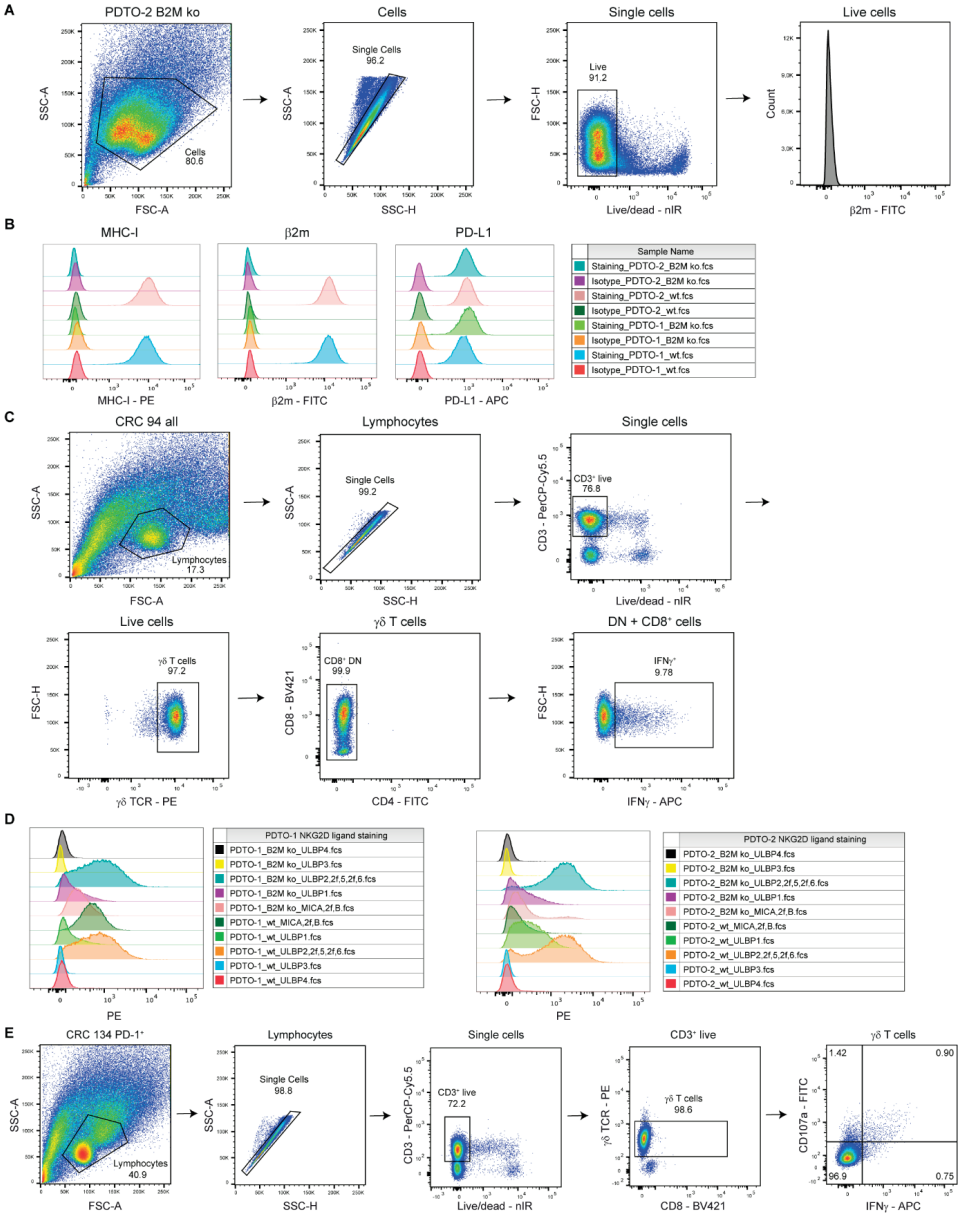

Figure S9. Reactivity of γδ T cells from MMR-d colon cancers towards cancer cell lines.
A. Flow cytometry gating strategy on PDTO cells for analysis of surface staining. Selected cells were gated on single, live cells before quantification of staining signal. **B**. Histogram representation and count for surface staining of MHC-I, PD-L1, and β2m expression on two PDTO lines *B2M*^{WT} and *B2M*^{KO} after IFN-γ pre-stimulation. Staining with isotype antibodies for each fluorochrome (PE, APC and FITC) were included as negative control. **C**. Flow cytometry gating strategy on γδ T cell samples for analysis of intracellular staining to test anti-tumor reactivity upon PDTO stimulation. Lymphocyte population was further gated on single cells, live and CD3^{+} cells, γδ TCR^{+} cells and CD8^{+} as well as CD8^{-} CD4^{-} cells. Reactivity of the sample was based on IFN-γ^{+} cells of the selected population. **D**. Histogram representation and count for surface staining of NKG2D ligands MICA/B, ULBP1, ULBP2/5/6, ULBP3, and ULBP4 on two PDTO lines *B2M*^{WT} and *B2M*^{KO} after IFN-γ pre-stimulation. **E**. Flow cytometry gating strategy on γδ T cell samples for analysis of intracellular staining after stimulation with PDTOs in the presence of NKG2D ligand blocking. Lymphocyte population

was further gated on single cells, live and CD3⁺ cells, followed by γδ TCR⁺ and CD8⁺ as well as CD8⁻ cells. Reactivity of final population was based on IFN-γ⁺ or CD107a⁺ cells.

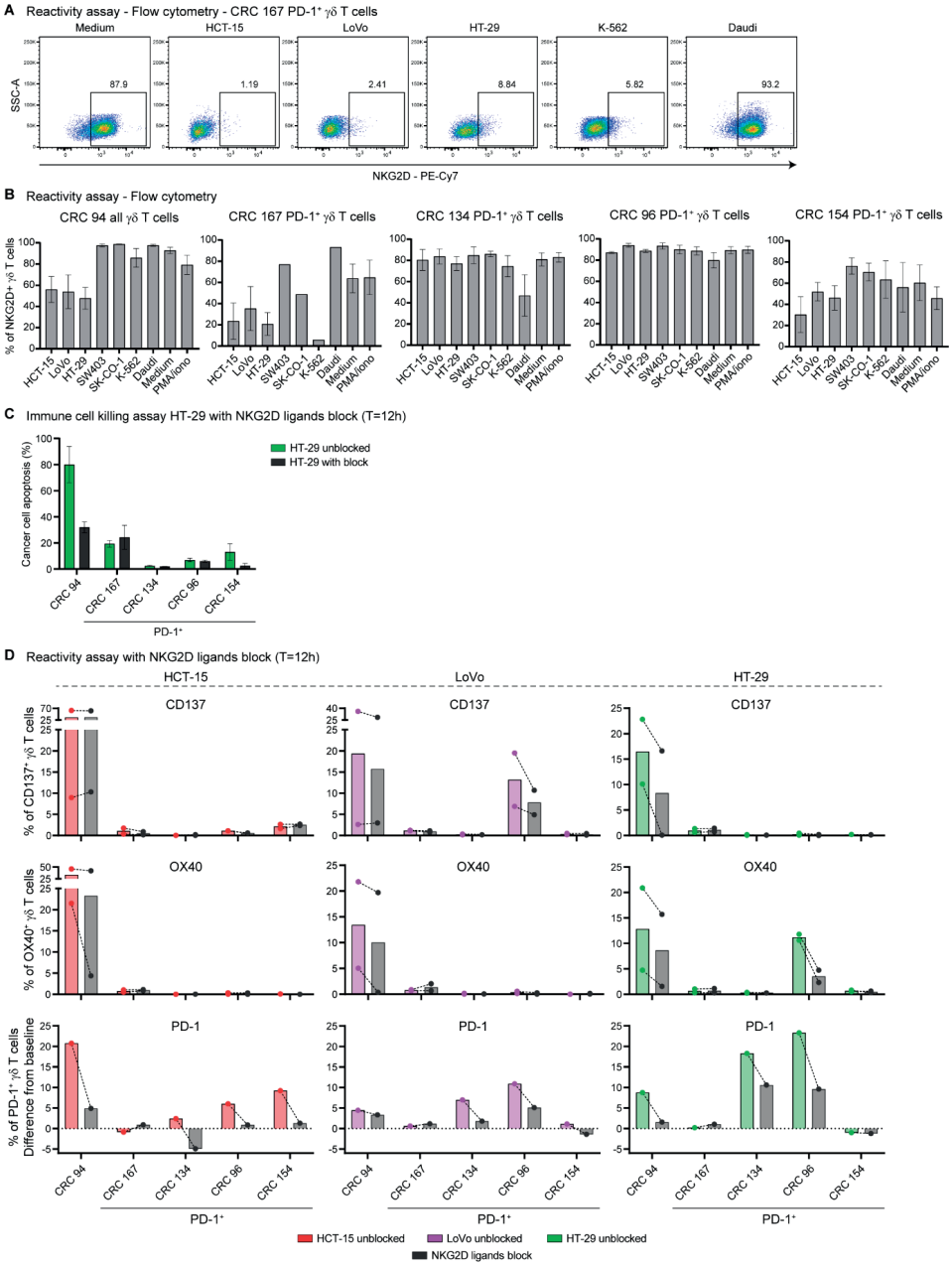

Figure S10. Reactivity towards and killing of cancer cell lines by PD-1⁺ γδ T cells from MMR-d colon cancers in the presence of NKG2D ligand blocking.

A. Representative flow cytometry plots showing the expression of NKG2D on PD-1⁺ γδ T cells from CRC167 after 18h co-culture with HCT-15, LoVo, HT-29, K-562, and Daudi cells as compared to medium only. Gates indicate percentage of positive γδ T cells. **B**. Bar plots showing the expression of NKG2D on PD-1⁺ γδ T cells from MMR-d colon cancers

(n=5) after 18h co-culture of PD-1⁺ γδ T cells with the cancer cell lines. Medium as negative control and PMA/ionomycin as positive control are included. Bars indicate mean ± SEM. Data from four (CRC94), three (CRC167, CRC96), or two (CRC134, CRC154) independent experiments, depending on availability of γδ T cells. **C**. Bar plots showing the quantification of killing of HT-29 cells by γδ d T cells from MMR-d colon cancers (n=5) in the presence of blocking antibodies for NKG2D ligands as compared to the unblocked condition after 12h co-culture. Bars indicate mean ± SEM of two wells with two images/well. **D**. Bar plots showing the percentage of CD137-positive (first row), OX40-positive (second row), and PD-1-positive (third row) γδ T cells after 18h co-culture of PD-1⁺ γδ T cells from MMR-d colon cancers (n=5) with HCT-15, LoVo, and HT-29 cells in the presence of blocking antibodies for NKG2D ligands. PD-1 expression is shown as difference from baseline (medium) condition. Bars indicate the mean and lines indicate similar experiments. Data from two independent experiments for CD137 and OX40.

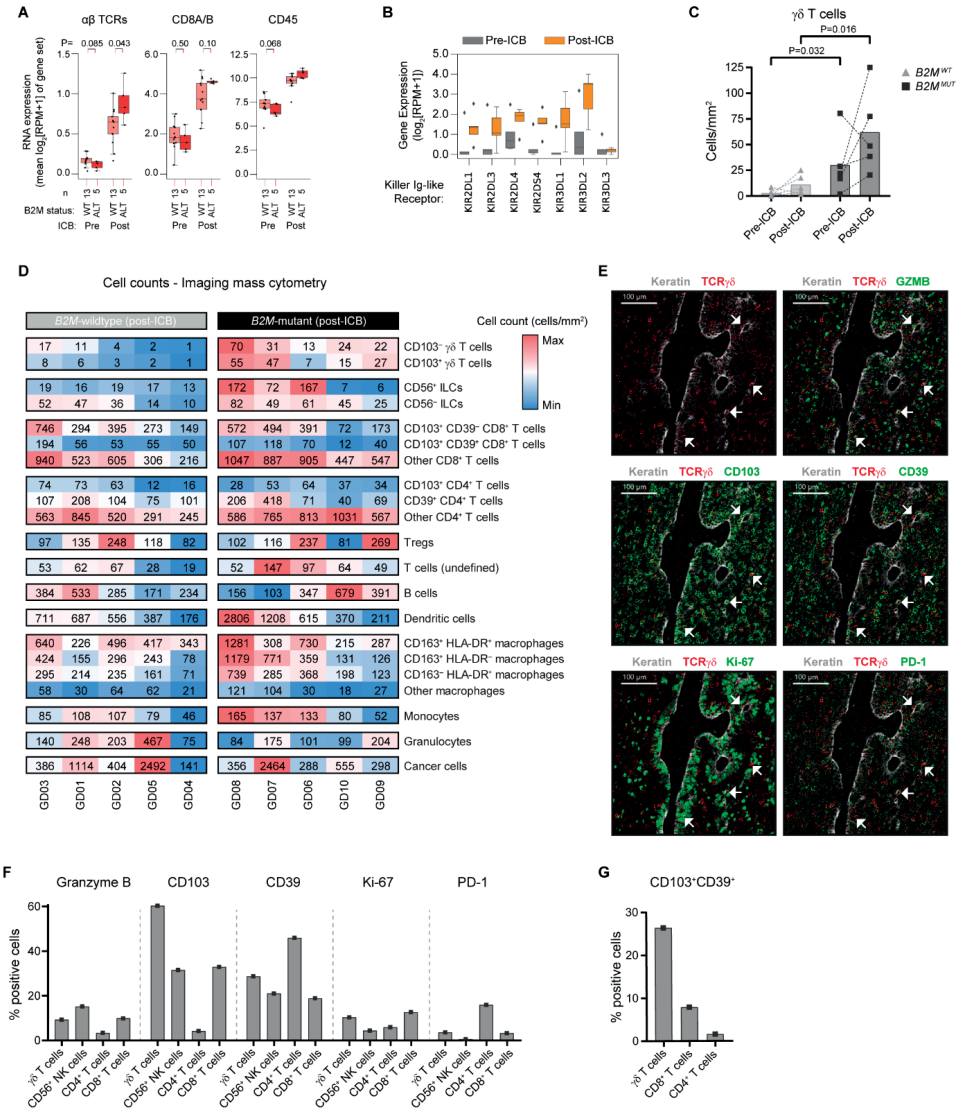

Figure S11. Distribution of immune cell populations in *B2M*-wildtype and *B2M*-mutant colon cancers upon immune checkpoint blockade (ICB) by imaging mass cytometry.

A. The RNA expression of different immune marker gene sets in MMR-d *B2M*^{WT} (pink), and MMR-d *B2M*^{MUT} (red)

cancers, before (left) and after (right) neoadjuvant ICB in the NICHE study. Boxes, whiskers, and dots indicate quartiles, 1.5 interquartile ranges, and individual data points, respectively. Wilcoxon rank sum test-based P-values are shown for MMR-d *B2M*^{WT} *vs* MMR-d *B2M*^{MUT} cancers. **B**. Boxplot showing the pre- (gray) and post-ICB (orange) RNA expression of killer-cell Ig-like receptors (KIRs) in MMR-d cancers in the NICHE study with high impact (inactivating) mutations in *B2M*. Boxes, whiskers, and dots indicate quartiles, 1.5 interquartile ranges, and outliers, respectively. P-values were calculated by Wilcoxon rank sum test. **C**. Frequencies of γδ T cells in *B2M*^{WT} (n=5) and *B2M*^{MUT} (n=5) MMR-d colon cancers pre- and post-ICB treatment corresponding to **Figure 4B** with lines indicating paired samples. Each dot represents an individual sample. P-values were calculated by Wilcoxon rank sum test. **D**. Table showing cell counts (cells/mm^2) of different (immune) cell types from the imaging mass cytometric detection of *B2M*^{WT} (n=5) and *B2M*^{MUT} (n=5) MMR-d colon cancers upon ICB treatment. Hierarchical clustering was performed on the samples within the two groups. Color bar is scaled per major immune lineage. **E**. Representative images of the detection of cytotoxic (granzyme B$^+$), tissue-resident (CD103$^+$), activated (CD39$^+$), proliferating (Ki-67$^+$), and PD-1$^+$ γδ T cells by imaging mass cytometry in a *B2M*^{MUT} MMR-d colon cancer upon ICB treatment. **F**. Frequencies of marker-positive γδ T cells, CD56$^+$ NK cells, CD4$^+$ T cells, and CD8$^+$ T cells in the sole *B2M*^{MUT} MMR-d colon cancer that contained cancer cells upon ICB treatment. **G**. Frequencies of CD103$^+$CD39$^+$ γδ T cells, CD8$^+$ T cells, and CD4$^+$ T cells in the sole *B2M*^{MUT} MMR-d colon cancer that contained cancer cells upon ICB treatment.

SUPPLEMENTAL TABLES AND MOVIES

The supplementary tables and movies are available in the appendix to this thesis at the repository of Leiden University (https://hdl.handle.net/1887/3439882) and can be requested from the author.

Table S1: Characteristics of clinical samples from 71 patients with MMR-d cancers from the DRUP study.
Table S2: Immune marker gene sets for bulk RNA-seq analyses.
Table S3: Characteristics of clinical samples from 17 patients with ICB-naïve MMR-d colon cancer.
Table S4: Characteristics of patient-derived organoids from MMR-d colorectal cancer.
Table S5: Antibodies used for imaging mass cytometry of colon cancers.
Table S6: Antibodies used for immunophenotyping of γδ T cells by flow cytometry.

Movie 1: Killing of HCT-15 cells by γδ T cells (Vδ1^{+}) from a MMR-d colon cancer.
Movie 2: Killing of HCT-15 cells by PD-1^{+} (Vδ1^{+}) as compared to PD-1^{-} (Vδ2^{+}) γδ T cells from a MMR-d colon cancer.